AIP | Physics of Fluids

Decomposition driven interface evolution for layers of binary mixtures. III. Two-dimensional steady films with flat and modulated surfaces

Fathi A. M. Bribesh, Ľubor Fraštia, and Uwe Thiele

Citation: Phys. Fluids **24**, 062109 (2012); doi: 10.1063/1.4727888
View online: http://dx.doi.org/10.1063/1.4727888
View Table of Contents: http://pof.aip.org/resource/1/PHFLE6/v24/i6
Published by the American Institute of Physics.

Decomposition driven interface evolution for layers of binary mixtures. III. Two-dimensional steady films with flat and modulated surfaces

Fathi A. M. Bribesh,[a] Ľubor Fraštia, and Uwe Thiele[b]
Department of Mathematical Sciences, Loughborough University, Loughborough, Leicestershire LE11 3TU, United Kingdom

(Received 18 January 2012; accepted 16 May 2012; published online 28 June 2012)

We study two-dimensional steady concentration and film thickness profiles for isothermal free surface films of a binary liquid mixture on a solid substrate employing model-H that couples the diffusive transport of the components of the mixture (convective Cahn-Hilliard equation) and the transport of momentum (Navier-Stokes-Korteweg equations). The analysis is based on minimising the underlying free energy equivalent to solving the static limit of model-H. Additionally, the linear stability (in time) of relevant layered films is analyzed. This allows for a comparison of the position of certain branching points in the bifurcation diagrams of steady solutions with the value predicted as onset of a linear instability. Results are presented for the cases of (i) a flat film without energetic bias at the free surface, (ii) a flat film with energetic bias, (iii) a height-modulated film without energetic bias, and (iv) a height-modulated film with energetic bias. In all cases we discuss symmetries of the various steady solutions allowing us to order them and to infer properties of solution branches and relations between them. © *2012 American Institute of Physics*. [http://dx.doi.org/10.1063/1.4727888]

I. INTRODUCTION

Layers, drops, and meniscii of simple and complex liquids with a free surface are increasingly important in many technological applications. They are employed, for instance, in the fabrication of advanced microelectronics (through immersion lithography), electrocatalysts and solar cells, they are important for lubrication and in fuel cells.[1–4] Another application is the use of liquid films as or in the production of protective and/or functional coatings that occurs in a number of natural and industrial processes. To understand and control such processes where films of simple and complex liquids play an important role, a profound knowledge of their static and dynamic properties is required. For complex fluids this includes their internal micro- and nano-structure. An interesting example for films of complex liquid are films of binary liquid mixtures located on solid substrates and open to the surrounding gas phase. They are, for instance, encountered at intermediate stages of the production process of functional polymer coatings of solid surfaces and also represent model systems for more complex mixtures employed in the production of organic solar cells. Motivated by the wide range of applications, a variety of films of polymer blends is investigated experimentally.[2,5–10]

For single films and drops of simple pure nonvolatile liquids on smooth homogeneous solid substrates, one has reached a relatively good understanding of their static and dynamic properties, e.g., in the context of dewetting.[11–13] However, in various applications the liquids of interest may consist of several components, may be volatile or rest on structured substrates. Alternatively several liquids are involved, e.g., in a multilayer film. All these additional effects may occur in various combinations, and result in more complex behaviour. Quite a number of fundamental questions are

[a]Electronic mail: f.bribesh@lboro.ac.uk. Present address: Department of Mathematics, Zawia University, Zawia, Libya.
[b]Electronic mail: u.thiele@lboro.ac.uk. URL: http://www.uwethiele.de.

not yet sufficiently understood for the amended systems. A particularly challenging aspect is related to the occurrence of free interfaces and wetting effects. For example, experiments with films of polymer blends find that phase enrichment at the boundaries and phase separation within the film are related to developing modulations of the free film surface, and even result in the dewetting of the film itself.[5,6,14] Not many approaches for the modelling of these phenomena exist: there are some studies that employ model-H in a film geometry (see below) (Refs. 15–17), and long-wave approaches[18] that result in a reduced description that is valid for predominantly laterally structured films.[19–21] For predominantly vertical structuring one may describe the late stages of evolution by two-layer long-wave models.[22–24]

Here we are mainly interested in the coupling of decomposition within a film of a binary liquid mixture and changes in the surface profile of the film. As a continuation of previous work,[15,17] we study free surface films of binary liquid mixtures on a horizontal homogeneous smooth solid substrate. The behaviour of these films is investigated in situations where the decomposition of the mixture into the two components may result in various concentration patterns and may also trigger a change in the film thickness profile. The resulting surface deflection will depend on the strength of the solutal Marangoni effect, i.e., on the contrast in the liquid-gas interface tension of the two individual components. If the resulting structuring is not predominantly lateral, i.e., if the concentration gradient differs significantly from being parallel to the solid substrate, one is in general not able to employ a long-wave approach and needs to consider the full hydrodynamic description. It corresponds to model-H (Refs. 25 and 26), which couples the transport of momentum (Navier-Stokes-Korteweg equations, i.e., Navier-Stokes equations with an additional contribution in the stress tensor, resulting from concentration gradients—the Korteweg stresses) and the transport of the mass of the components (convective Cahn-Hilliard equation). It is studied in different (possibly non-isothermal) settings[26–32] (see also references in Ref. 15). The major part of the literature focuses on a bulk situation, i.e., it does not consider situations like a film of a mixture that involve beside the internal diffuse interfaces a free liquid-gas interface.

The present work forms the third part of a sequence of papers dedicated to the development and application of model-H in the presence of free surfaces. This necessarily implies the incorporation of hydrodynamic flow even if it is extremely slow creeping flow. Without such a flow, e.g., with a description based solely on the Cahn Hilliard equation,[33] one is not able to describe an evolving surface profile. The present part (III) analyzes fully two-dimensional steady film states and builds on part (I) (Ref. 15) and part (II) (Ref. 17) that are respectively dedicated to one-dimensional steady states, i.e., steady stratified (layered) films and their linear stability with respect to lateral instability modes. Note that Ref. 15 starts by deriving a generalized model-H employing phenomenological non-equilibrium thermodynamics. The model consists of coupled transport equations for density, momentum, and entropy. For an isothermal setting, zero interface viscosity, and a simplified double-well internal energy, the general model simplifies to a form of model-H that may be compared to literature results. The comparison allows for a clarification of issues related to the definitions of pressure and chemical potential. Furthermore, boundary conditions at the solid substrate and the free interface are introduced. After non-dimensionalization, the relation between the respective dimensionless numbers entering the boundary conditions for the Cahn-Hilliard (concentration) and the Navier-Stokes-Korteweg (momentum) equations are discussed. It is clarified that the energetic bias with respect to decomposition at a free surface is intrinsically coupled to a solutal Marangoni effect implying that neither of the two effects should be considered without the other one present.[15] Our approach differs from the one taken in Ref. 16, where the two boundary conditions are treated as independent. The linear stability analysis of part (II) (Ref. 17) focuses on the stability of homogeneous and layered films [determined in part (I)] with respect to modulations in thickness and/or composition along the substrate. Thereby, neutral and energetically biased free surfaces are considered and the influence of the mean composition is discussed.

The present paper determines various fully two-dimensional steady film states that are characterized by non-uniform concentration profiles within the film and a free surface that can be flat or curved. The numerical tools employed are presented in Ref. 34. The analysis is performed with and without energetic bias at the free surface. The paper is organised as follows. In Sec. II we briefly recapitulate the non-dimensional model-H, the appropriate boundary conditions, the

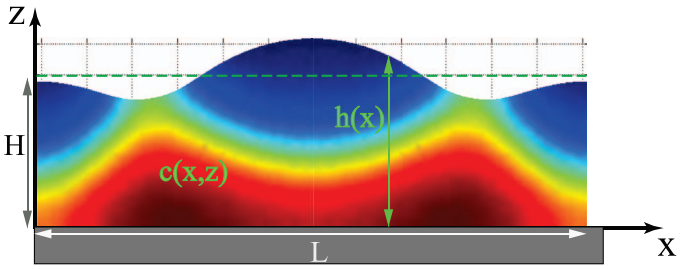

FIG. 1. Sketch of the two-dimensional (2D) geometry: an infinitely extended free-surface film of a liquid binary mixture on a horizontal smooth solid substrate.

linearization of the fully time-dependent equations about the stratified steady films and the employed numerical schemes. Using the parameters for polymer blends as in Ref. 17, Secs. III and IV discuss the linear stability of homogeneous films and the 1D (layered) film states, respectively. The following Sec. V analyzes fully two-dimensional steady film states and relates their features to the results of the linear stability analysis. In particular, we present results for the cases of (i) a flat film without energetic bias at the free surface (Sec. V A), (ii) a flat film with energetic bias (Sec. V B), (iii) a height-modulated film without energetic bias (Sec. V C), and (iv) a height-modulated film with energetic bias (Sec. V D). Note that here the influence of the composition of the film is not discussed as we focus on the "critical case", i.e., a symmetric blend where the concentrations of the two components are equal. The "off-critical case", i.e., of a non-symmetric blend where the concentrations of the two components are not equal, is considered elsewhere.[35] Finally, conclusions are given in Sec. VI.

II. MODEL AND NUMERICAL PROCEDURE

As the present work is part of a sequence of papers, we keep the description of the model brief. A re-derivation of model-H, its dimensional form in the isothermal case (including boundary conditions at the free surface and the solid substrate), and details of its non-dimensionalization are detailed in Ref. 15 where the used model-H is also compared to other forms in the literature.[25–29] Here we only introduce the non-dimensional model and discuss the relevant non-dimensional parameters.

The stability of stratified solutions (layered films) with respect to lateral harmonic perturbations of the concentration and film thickness profile is discussed in detail in Ref. 17, whereas the numerical method to obtain fully two-dimensional steady state solutions is introduced in Ref. 34.

A. Model-H

The time evolution of a binary fluid mixture in an isothermal situation is often described by model-H. This short name (introduced in Ref. 25) stands for a coupled system of kinetic equations describing the transport of momentum and of some conserved scalar field (that in our case is concentration) (Ref. 26). The Navier-Stokes description of a simple fluid is supplemented by an additional contribution to the stress tensor that depends on concentration gradients and is sometimes called Korteweg stress.[36] Such a model-H was re-derived in Ref. 15 in the general non-isothermal case, and then employed in the isothermal case that we also consider here. For a two-dimensional (2D) setting (see Fig. 1), the non-dimensional transport equation of momentum is

$$\mathrm{Ps}\left[\frac{\partial \mathbf{v}}{\partial t} + \mathbf{v}\cdot\nabla\mathbf{v}\right] = -\nabla\cdot\left\{(\nabla c)(\nabla c) + p_{\mathrm{eff}}\underline{\mathbf{I}}\right\} + \frac{\mathrm{Ps}}{\mathrm{Re}}\Delta\mathbf{v}, \tag{1}$$

where we have assumed that the density of the mixture is independent of the mixture composition implying that continuity gives $\nabla\cdot\mathbf{v} = 0$. Here, $\mathbf{v} = (u, w)$ is the velocity field, $c = c_1 - c_2 = 2c_1 - 1$ is the concentration field defined as the difference of the concentrations of the two components, the effective pressure $p_{\mathrm{eff}} = p - (c+1)\Delta c - (\Delta c)^2/2$ contains all diagonal terms of the stress tensor where p is the "usual" pressure, and the dimensionless numbers Ps and Re are discussed below.

Equation (1) is coupled to a Cahn-Hilliard description[33,37] of the binary mixture supplemented by a term that describes advective transport with the velocity $\mathbf{v} = (u, w)$:

$$\partial_t c + \mathbf{v} \cdot \nabla c \; = \; -\nabla \cdot \{\nabla[\Delta c - \partial_c f(c)]\}\,, \tag{2}$$

The 2D operators are $\nabla = (\partial_x, \partial_z)$ and $\Delta = \left(\partial_x^2 + \partial_z^2\right)$, and the function $\partial_c f(c)$ is a chemical potential related to the local bulk free energy $f(c)$ that here corresponds to the simple quartic potential $f(c) = (c^2 - 1)^2/4$. In order to obtain the non-dimensional form of the governing equations [Eqs. (1) and (2)], in Ref. 15 the scales $l = C\sqrt{\sigma_c/E}$, $U = M\,E/(l\,C^2)$, $\tau = l/U = l^2\,C^2/(ME)$, and $P = E$ are introduced for length, velocity, time, and pressure, respectively. Thereby the length l represents the thickness of the diffuse interface between the two phases of the mixture and is determined from σ_c (interfacial stiffness of the diffuse interface), the energy scale E and the concentration C at the binodal; M is the mass diffusion coefficient or diffusional mobility.

With these scales, two dimensionless numbers appear in the bulk Eqs. (1) and (2), the pressure number $\mathrm{Ps} = \rho\,\mathrm{M}^2\,E^2/\mathrm{C}^6\,\sigma_c$ and the Reynolds number $\mathrm{Re} = \mathrm{M\,E}\rho/\eta\,C^2$. As the diffusion constant is $D = ME$ and $U \sim D/l$, the used Reynolds number can be seen as an inverse Schmidt number $\mathrm{Sc} = \eta/\rho D$. The ratio $\mathrm{Re/Ps}=\sigma_c C^4/\eta ME$ turns out to be the most important bulk parameter for the extremely slow creeping flow we are interested in: For films of decomposing polymer mixtures,[5] Re, Ps $\ll 1$, but $\mathrm{Re/Ps} = O(1)$ (see Sec. III C 2 of Ref. 17). It corresponds to the ratio of the typical velocity $U' = \sigma/\eta$ of the viscous flow driven by the internal "diffuse interface tension" $\sigma = \sigma_c/l$ and the typical velocity of diffusive processes $U \sim M\,E/l = D/l$. This implies that Re/Ps can as well be seen as a Peclet number $\mathrm{Pe}=U'l/D$ or as an inverse Capillary number $\mathrm{Ca}^{-1} = \sigma/U\eta$. Such alternative scalings are used, for instance, in Refs. 29 and 30.

Equations (1) and (2) are supplemented by boundary conditions for the concentration and velocity fields at the solid substrate ($z = 0$) and the free sharp liquid-gas interface ($z = h(x, y, t)$). At $z = 0$, one imposes (i) zero diffusive mass flux through the substrate and (ii) energetic neutrality (i.e., the substrate does not prefer any of the two components; cf. Ref. 15 for other cases), i.e.,

$$\partial_z\,[(\partial_{xx} + \partial_{zz})c - \partial_c f(c)] = 0, \tag{3}$$

$$\partial_z c = 0, \tag{4}$$

respectively. As a result the diffuse interface between the two components meets the solid surface at a right angle. For the velocity field the (iii) no-slip and (iv) no-penetration conditions hold, i.e., $v = w = 0$. At the free surface ($z = h(x, y, t)$), similar conditions hold for the concentration field: (v) zero diffusive through flux

$$[\partial_z - (\partial_x h)\partial_x]\,[(\partial_{xx} + \partial_{zz})c - \partial_c f(c)] = 0, \tag{5}$$

and (vi) an energetic bias of the free surface towards one of the two components

$$[\partial_z - (\partial_x h)\partial_x]\,c + \mathrm{S}\partial_c f^+(c)\sqrt{1 + (\partial_x h)^2} = 0. \tag{6}$$

The dimensionless $\mathrm{S} = \gamma_0/l\,E$ represents the ratio of the surface tension of the free surface γ_0 at $c = 0$, and the interface tension of the diffuse interface lE. We consider a linear dependence of surface energy f^+ on concentration

$$f^+(c) = \alpha + a^+ c, \tag{7}$$

i.e., for $a^+ = 0$ the surface is neutral, whereas for $a^+ > 0$ an energetic bias results in preferential adsorption of component two. Note that the linear bias corresponds to a linear Marangoni effect. The case $a^+ > 0$ with an energetically neutral solid substrate is in Refs. 15 and 17 called the case of asymmetric bias. Note that α is only used to "switch" between the cases of a film that can freely change its thickness profile ($\alpha = 1$), and a film that has a flat surface ($\alpha \gg 1$). In the numerical calculations for the latter case, we use $\alpha = 10^3$. The conditions for the velocity field result from the

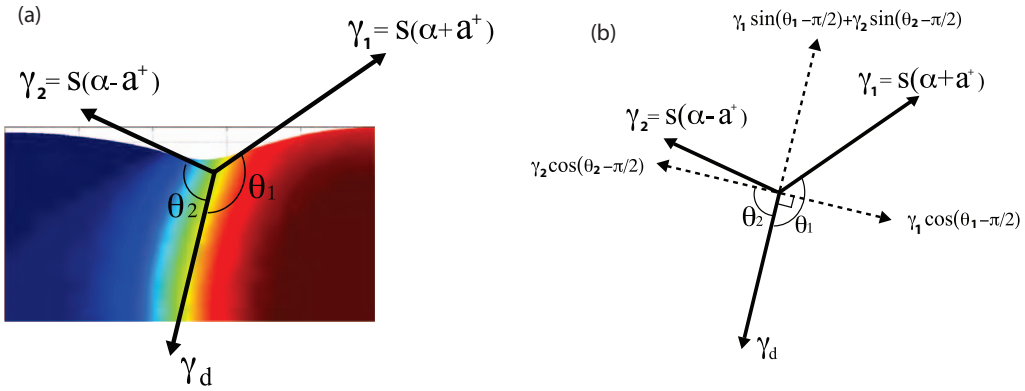

FIG. 2. Panel (a) shows the profile of the surface modulated film (1/2, 0) with energetic bias at the free surface with the forces acting at the contact point. It also indicates the definitions of the non-dimensional tensions γ_1, γ_2 and $\gamma_d = 1$. Panel (b) shows the projection of the forces onto perpendicular directions.

(vii) balance of tangential forces

$$\begin{aligned} &- [\partial_x c + (\partial_x h)\partial_z c]\,[\partial_z c - (\partial_x h)\partial_x c] \\ &+ \frac{\mathrm{Ps}}{\mathrm{Re}}\left[(u_z + w_x)(1 - h_x^2) + 2(w_z - u_x)h_x\right] \\ &= \mathrm{S}\sqrt{1 + h_x^2}\,[\partial_x + (\partial_x h)\partial_z]\, f^+(c) \end{aligned} \tag{8}$$

and (viii) balance of normal forces

$$\begin{aligned} &- \frac{1}{1 + h_x^2}\,[\partial_z c - (\partial_x h)\partial_x c]^2 - p_{\mathrm{eff}} \\ &+ \frac{\mathrm{Ps}}{\mathrm{Re}}\frac{2}{1 + h_x^2}\left[u_x h_x^2 + w_z - h_x(u_z + w_x)\right] \\ &= \mathrm{S} f^+(c)\partial_x\left[\frac{\partial_x h}{(1 + h_x^2)^{1/2}}\right]. \end{aligned} \tag{9}$$

Notice that the tangential gradient of $f^+(c)$ enters the tangential force balance corresponding to a solutal Marangoni force. The final condition is (ix) the kinematic condition

$$\partial_t h = w - u\partial_x h, \tag{10}$$

which ensures that the free surface follows the velocity field.

To get an estimate for the angles θ_1 and θ_2 between the diffuse interface separating two fluids and the left and the right part of the sharp free surface (see Fig. 2), respectively, one may employ an estimate within the sharp interface limit. In the case without energetic bias (where $\theta_1 = \theta_2 = \theta$) one finds the dimensionless expressions $\cos(\theta) = -1/2S$, i.e., $\theta = 2\pi/3$ for $S = 1$, while with energetic bias ($a^+ \neq 0$), the equilibrium of interfacial forces gives the following two equations:

$$\gamma_d = -\gamma_1 \cos\theta_1 - \gamma_2 \cos\theta_2, \tag{11}$$

$$\gamma_1 \sin\theta_1 = \gamma_2 \sin\theta_2. \tag{12}$$

Solving Eq. (11) and Eq. (12) for θ_1 and θ_2, one obtains the general relation

$$\cos\theta_1 = \frac{\gamma_2^2 - \gamma_1^2 - \gamma_d^2}{2\gamma_1\gamma_d} = \frac{-4S^2\alpha a^+ - \gamma_d^2}{2S\gamma_d(\alpha + a^+)}, \tag{13}$$

$$\cos\theta_2 = \frac{\gamma_1^2 - \gamma_2^2 - \gamma_d^2}{2\gamma_2\gamma_d} = \frac{4S^2\alpha a^+ - \gamma_d^2}{2S\gamma_d(\alpha - a^+)}. \tag{14}$$

For our case of a modulated free surface with $\alpha = 1$ and $\gamma_d = 1$, we have

$$\cos\theta_1 = -\frac{1 + 4S^2 a^+}{2S(1 + a^+)}, \tag{15}$$

$$\cos\theta_2 = -\frac{1 - 4S^2 a^+}{2S(1 - a^+)}. \tag{16}$$

However, for an imposed flat surface ($\alpha \gg 1$) with $\gamma_d = 1$, the relations become $\cos\theta_1 = -2Sa^+$ and $\cos\theta_2 = 2Sa^+$. Below, these relations will be checked against our diffuse interface results.

B. Two-dimensional steady states

Steady states, i.e., time-independent concentration and film thickness profiles can be obtained as solutions of the static limit ($\mathbf{v} = 0$, $\partial_t c(x, z) = 0$, $\partial_t h(x) = 0$) of the bulk Eqs. (1) and (2) and the boundary conditions (i)–(ix). The resulting system of equations can alternatively be derived by minimizing the energy functional

$$\begin{aligned} F[c(x,z), h(x), \lambda_d, \lambda] = {} & F_b[c(x,z), h(x), \lambda_d, \lambda] \\ & + F_s[c(x, h(x)), h(x)] \end{aligned} \tag{17}$$

with respect to variations of c and h at given liquid volume V (Lagrange multiplier λ) and mass of component one VC_1 (multiplier λ_d, see appendix of Ref. 15). Here,

$$\begin{aligned} F_b = {} & \int_{-\infty}^{\infty}\int_0^{h(x)} \left[\frac{1}{2}(\nabla c)^2 + f(c) - \lambda_d c_1 - \lambda\right] dz\,dx \\ & + \lambda_d C_1 V + \lambda V \end{aligned} \tag{18}$$

and

$$F_s = \mathrm{S}\int_{-\infty}^{\infty} f^+(c)\sqrt{1 + (\partial_x h)^2}\,dx \tag{19}$$

are the bulk and surface contributions, respectively. In the following, we obtain steady film thickness and concentration profiles by numerical determination of the extrema and saddles of the energy (17). Instead of a laterally infinite domain, the film is assumed to rest on a substrate of finite length L with von Neumann (no flux) boundary conditions at the lateral boundaries. Note that such a system can always be embedded in a periodic domain with the period equal to $2L$ (Ref. 38). The 2D steady states are found employing the Finite Element Method on an adaptive mesh as was developed in Ref. 34. It uses isoparametric linear triangular elements with area coordinates thereby mapping the physical film domain onto a rectangular numerical domain.[39] The adaptive mesh refinement improves the resolution in zones of high concentration gradients. The resulting system of algebraic equations is solved iteratively using a variable number of Newton steps. A simple numerical scheme is used to follow solution branches when changing some control parameter, e.g., the domain size L or the mean film thickness H. Various starting solutions are employed, e.g., homogeneous films with an imposed small noise in concentration, different films with weak layered or checkerboard concentration modulations. Note that the scheme is not able to follow solution branches around saddle-node bifurcations, i.e., points on the solution branch where the slope is infinite cannot be passed. This makes the procedure sometimes tedious, in particular, in parameter regions where there exist several steady solutions close to each other.

Additionally, a second approach is used for one-dimensional (1D) steady states, i.e., stratified flat layers where the concentration only depends on the z-coordinate.[15] The resulting equation for the concentration field $c(z)$ is solved using arc length continuation for ordinary differential equations based on Newton and Chord iterative methods as provided by the package AUTO (Ref. 40). This

allows us to obtain all relevant families of 1D solutions and to track their bifurcations in a similar way as is often done for thin film equations that are also of Cahn-Hilliard type.[12] The stratified solutions are obtained independently with both approaches and agree very well.

C. Linear stability analysis

The determination of 1D and 2D steady states described above is based on a solution of the static limit of the bulk equations of model-H (1) and (2). Although, here we do not study the fully nonlinear behaviour in time through a simulation of Eqs. (1) and (2), we accompany the static considerations by a linear stability analysis (in time). In this way one obtains information about the most dangerous instability modes and their growth rates.

To do so one linearizes Eqs. (1) and (2) about steady state solutions. Here, this is done (i) analytically for homogeneous films (see Sec. III below), numerically for steady stratified flat films, i.e., for concentration profiles $c_0(z)$, velocity $\mathbf{v}_0 = 0$, pressure $p_0(z) = (\partial_z c_0)^2$, and film thickness $h_0 = H$. We investigate their linear stability with respect to lateral perturbations of wavenumber k and growth rate β. A normal mode ansatz for the perturbations $(\tilde{\mathbf{v}}_1, \tilde{p}_1, \tilde{c}_1, \tilde{h}_1) = (\mathbf{v}_1(z), p_1(z), c_1(z), h_1)\exp(\beta t + ik_x x)$ (where fields $\epsilon\tilde{\mathbf{v}}_1$, $\epsilon\tilde{p}_1$, $\epsilon\tilde{c}_1$, and $\epsilon\tilde{h}_1$ denote the infinitesimal perturbations of velocity, pressure, concentration, and thickness fields, respectively, and k_x is the lateral wave-number) is introduced into Eqs. (1) and (2) and the boundary conditions. The system of equations is linearized in ϵ, the pressure is eliminated and the linearized model-H is written as an eigenvalue problem[17]

$$\begin{aligned}\partial_{zzzz} w_1 &= \beta\,\mathrm{Re}\,(\partial_{zz} - k_x^2)w_1 + \frac{\mathrm{Re}}{\mathrm{Ps}}\,k_x^4\,c_1\partial_z c_0 \\ &\quad - \frac{\mathrm{Re}}{\mathrm{Ps}}\,2k_x^2\partial_z[(\partial_z c_0)(\partial_z c_1)] \\ &\quad + \frac{\mathrm{Re}}{\mathrm{Ps}}\,k_x^2\partial_{zz}(c_1\partial_z c_0) + 2k_x^2\partial_{zz} w_1 - k_x^4 w_1 \end{aligned} \tag{20}$$

and

$$\begin{aligned}\partial_{zzzz} c_1 &= -(\beta c_1 + w_1\partial_z c_0) - (k_x^4 - 2k_x^2\partial_{zz})c_1 \\ &\quad + (\partial_{zz} - k_x^2)(c_1\partial_{cc} f|_{c_0}). \end{aligned} \tag{21}$$

The linearized boundary conditions are given in Sec. III B of Ref. 17. Note that Eqs. (20) and (21) are similar in form to the Orr-Sommerfeld equation. The base states $c_0(z)$ and solutions $c_1(z)$, $w_1(z)$, β of the eigenvalue problem are all obtained employing the numerical continuation algorithms of AUTO (Ref. 40). In a typical set of runs, one starts from the trivial solution at $a^+ = 0$: $c_0(z) = 0$, finds the layered steady states that bifurcate from the trivial one, increases the energetic bias at the free surface, finds a real eigenvalue β for a given wavenumber k_x as branching point, and in a final continuation step directly follows the dispersion relation $\beta(k_x)$ (Ref. 17).

D. Solution measures

We characterize the steady states by the normalized L_2-norm of the concentration field

$$||\delta c|| = \sqrt{\frac{1}{L\bar{h}}\int_0^L \int_0^{h(x)} \left(c(\mathbf{x}) - \bar{c}\right)^2 dz dx}, \tag{22}$$

the normalized L_2-norm of the film thickness profile

$$||\delta h|| = \sqrt{\frac{1}{L}\int_0^L \left(h(x) - \bar{h}\right)^2 dx}, \tag{23}$$

and the normalized energy

$$E = \frac{1}{L}\int_0^L \left\{(a^+c)\sqrt{1+(\partial_x h)^2} + \int_0^{h(x)} \left[\frac{1}{2}(\nabla c)^2 + f(c)\right] dz\right\} dx - \mathbf{a}. \tag{24}$$

Note that the c-independent part of the surface energy f^+ [Eq. (7)] is not included for a flat interface. For a modulated surface only the deviation from the energy of a flat surface enters E. Neither is the constant energy of the liquid-substrate interface. In consequence, the present energies for the case of a flat film differ from the ones in Ref. 15 by an offset of -2. Finally, $f(c)$ is the bulk energy introduced in Sec. II A. Here we use the simple quartic polynomial

$$f(c) = \frac{1}{4}(c^2-1)^2. \tag{25}$$

In this way, the surface deflection is measured by $||\delta h||$ and the strength of decomposition by $||\delta c||$. For flat films $||\delta h|| = 0$, whereas for homogeneous films $||\delta c|| = 0$. The energy E measures the difference to a homogeneous film at equilibrium concentration $c = \pm 1$.

All calculated film states are further characterized by their (conserved) volume $V = HL$, where H is the mean film thickness and L is the lateral domain size. In our bifurcation diagrams the lateral domain size L is used as control parameter whereas H is fixed at particular values. Note that the thickness profile $h(x)$ is part of the result as well as the concentration profile $c(x, z)$. In the present work, we only treat the case of a critical mixture, i.e., the mean concentration is $\bar{c} = 0$. For the off-critical case, see Ref. 35.

In the following we distinguish four main cases and discuss them for a number of mean film heights. In particular, we study flat and modulated films without and with energetic bias at the free surface. We choose $a^+ > 0$, i.e., the free surface prefers component two that dominates where $c < 0$. For critical concentration ($\bar{c} = 0$), the case $a^+ < 0$ is related by symmetry. Before we report on the fully nonlinear results for the one-dimensional case in Sec. IV and the two-dimensional case in Sec. V, we discuss in Sec. III the linear stability of a flat homogeneous film.

III. LINEAR STABILITY OF HOMOGENEOUS FILMS

Homogeneous films ($c_0 = 0$) are steady solutions only in the case without energetic bias, $a^+ = 0$. Inspection of the linearized Eqs. (20) and (21) shows that for $c_0 = 0$ the perturbations in the concentration and in the velocities decouple, i.e., advection does not influence the evolution in the linear stage. As all the velocity modes are stable one only needs to consider instability modes of the concentration field that are described by Eq. (21) with $c_0 = 0$:

$$\partial_{zzzz} c_1 = -\beta c_1 - (k_x^4 - 2k_x^2\partial_{zz})c_1 - (\partial_{zz} - k_x^2)c_1. \tag{26}$$

The boundary conditions are at $z = 0$ and $z = h_0$

$$\partial_z c_1 = \partial_{zzz} c_1 = 0. \tag{27}$$

In consequence of the decoupling no surface deflections can develop in the linear stage. All unstable modes are purely diffusive and similar to the ones obtained in a Cahn-Hilliard model for decomposition in a finite gap.[17,41]

To solve Eq. (26) with Eq. (27) one may use a harmonic ansatz not only for the lateral but also for the vertical spatial dependence, i.e., $c_1(z) = \epsilon \exp(ik_z z)$, where k_z is the real vertical wavenumber. After linearization in ϵ one obtains the dispersion relation

$$\beta = -\left[k_x^2 + k_z^2\right]\left[k_x^2 + k_z^2 - 1\right], \tag{28}$$

i.e., the film is unstable ($\beta > 0$) for modes with $k_x^2 + k_z^2 < 1$. For finite domains it is convenient to introduce vertical and lateral mode numbers $n = k_z H/2\pi$ and $s = k_x L/2\pi$, respectively. For the employed boundary conditions, n and s can take integer and half-integer values.

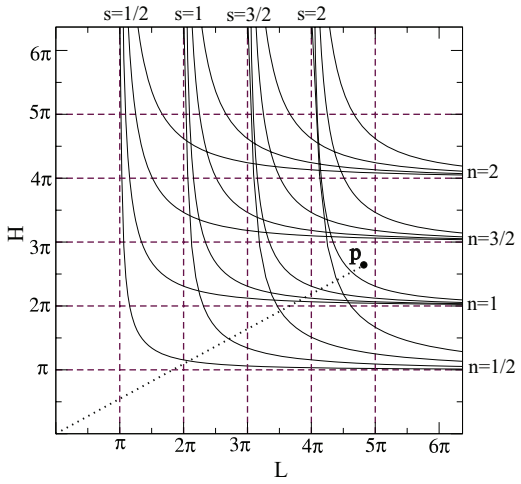

FIG. 3. Linear stability thresholds for and loci of symmetry breaking bifurcations from the trivial homogeneous flat film state (without energetic bias, $a^+ = 0$) as a function of the domain size L and the film thickness H. The horizontal and vertical dashed lines represent thresholds for vertical structuring, i.e., $(0, n)$ modes, and lateral structuring, i.e., $(s, 0)$ modes, respectively. The solid lines correspond to checker-board modes (s, n) with $s, n = 1/2, 1, 3/2, 2$. The mean concentration is $\bar{c} = 0$. The number of unstable modes for a given pair L and H is obtained by counting the number of thresholds one crosses when moving on a straight line from the corresponding point P in the (L, H)-plane to the origin. The example for P in the figure corresponds to 14 unstable modes.

First, we fix the mode number in the vertical direction to $n = 0$, i.e., we have $k_z = 0$ and purely lateral structuring with mode numbers $s = 1/2, 1, 3/2, \ldots$ above critical domain sizes $L_s^{ls} = 2\pi s$. Similarly, for $s = 0$ one has $k_x = 0$ and obtains purely vertical structuring (layered films) with mode numbers $n = 1/2, 1, \ldots$ above critical film heights $H_n^{vs} = 2\pi n$. Finally, the homogeneous film is unstable with respect to checkerboard modes, i.e., $s \neq 0$ and $n \neq 0$, for

$$L_{s,n}^{\mathrm{cb}} = \frac{sH}{\sqrt{(H/2\pi)^2 - n^2}}, \tag{29}$$

where we have used the mean film thickness as parameter. The number of unstable modes for certain film thicknesses H and domain sizes L can be obtained from Fig. 3 where the linear stability thresholds for the various modes are given. Note that the stability thresholds for vertical, lateral, and checkerboard modes also correspond to loci of symmetry breaking pitchfork bifurcations where branches of vertically structured (layered), laterally structured, and checkerboard steady solutions bifurcate from the trivial homogeneous solution. In the following, we will denote both, the linear modes and the fully nonlinear solutions branching of the trivial solution, by their corresponding pair of mode numbers (s, n).

Next, we discuss results for 1D steady states that correspond to layered 2D states (Sec. IV) and fully 2D steady states together with the linear stability of the relevant layered states (Sec. V). We work with a small number of fixed mean film heights, $H = 2.5$, $H = 3.5$, and $H = 5$, and use the energetic bias a^+ (in 1D) and the domain size L (in 2D, at various fixed a^+) as control parameters.

IV. ONE-DIMENSIONAL CASE—STRATIFIED FILMS

Before we embark on the study of fully 2D solutions, we discuss the possible stratified states, i.e., layered flat films without any lateral structure. They are studied in detail in Ref.15. We briefly review the cases of neutral and asymmetrically biased free surface that are relevant here.

Depending on the film thickness, homogeneous films may demix into a number of different stratified states that can be characterized by the norm of the concentration profile (Fig. 4) and energy (Fig. 5). Normally, the energy of the solutions is higher for a larger number of layers, i.e., multilayer film states occur in the time evolution as transients only. The thicker the films, the more layered

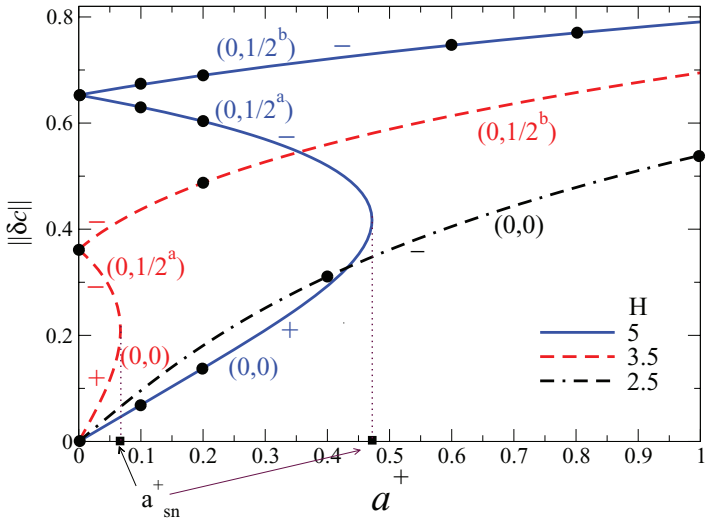

FIG. 4. Branches of steady vertical concentration profiles for layered films with biased free surface ($a^+ \geq 0$) of a critical mixture $\bar{c} = 0$ in dependence of a^+. The thicknesses are $H = 2.5$ [dot-dashed line (black online)], $H = 3.5$ [dashed line (red online)], and $H = 5$ [solid line (blue online)]. The vertical dotted lines indicate the location of the saddle-node bifurcation points. The black dots indicate solutions at particular values of a^+ that are further discussed later on. The symbols "+" and "−" indicate linear instability and stability with respect to one-dimensional perturbations, respectively.

states exist. In the neutral case subsequent layered states branch off the trivial state at $H = 2n\pi$ (cf. Sec. III). For $\bar{c} = 0$ all bifurcations are supercritical. Note that $2n + 1$ corresponds to the number of layers: $n = 1/2$ is a two-layer state, $n = 1$ is a three layer state, i.e., a sandwich structure.

Particularly interesting are the two-layer and the sandwich structure. For $H < 3\pi$, they are the only nontrivial solutions. In Fig. 4, the trivial ($n = 0$) and the two-layer ($n = 1/2$) state for a neutral surface are indicated by the black dots at $a^+ = 0$. The $n = 1/2$ solution is not present for $H = 2.5 < \pi$. For $H = 3.5$ and $H = 5.0$, it actually represents two solutions called $n = 1/2^a$ and $n = 1/2^b$. They are related by the symmetries $z \to H - z$ and $c \to -c$ and can therefore not be distinguished by global measures like the energy or norm. In the context of two-dimensional states, we call the

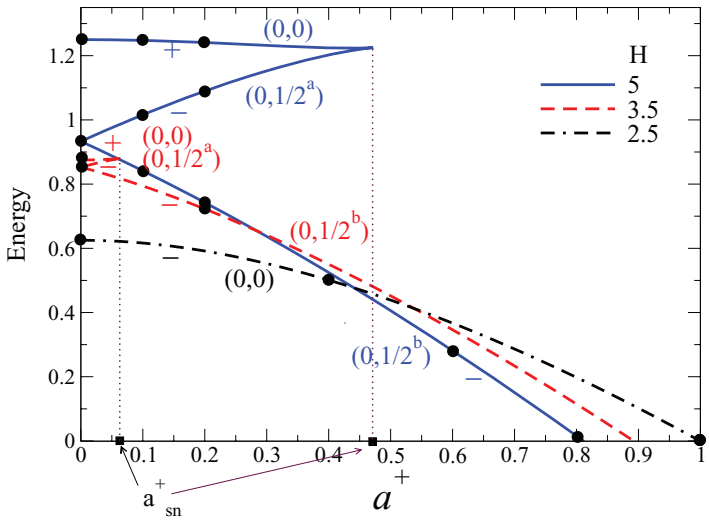

FIG. 5. Branches of steady layered films of critical mixture $\bar{c} = 0$ are characterized by their energy in dependence of the bias $a^+ \geq 0$ at the free surface. Film heights and symbols are as in Fig. 4.

stratified, laterally homogeneous films (0, n) branches, where the zero corresponds to the lateral mode number s.

Introducing the energetic bias ($a^+ > 0$) breaks the symmetry between the two $n = 1/2$ solutions as now component two is preferred at the free surface. This implies that for $a^+ > 0$ two branches emerge from the single $n = 1/2$ dot at $a^+ = 0$. The $n = 1/2^b$ branch is the one of the two that is more relevant. It has component two at the free surface and is therefore of lower energy (and larger norm) than the $n = 1/2^a$ branch that has component one at the free surface. Note, however, that both branches are linearly stable in 1D. The $n = 1/2^b$ branch has a norm (energy) that monotonically increases (decreases) with increasing bias. For $a^+ > 0$, the homogeneous $n = 0$ state does not exist anymore as such. Component one is enriched at the surface and the norm increases from zero. We call this a weakly stratified film. The enrichment layer becomes more pronounced with increasing bias. The state is, however, linearly unstable even in 1D and the corresponding branch annihilates with the $n = 1/2^a$ branch in a saddle-node bifurcation at a^+_{sn}. For $H = 2.5$, the weakly stratified layer is stable and has component two enriched at the surface (cf. also Fig. 10 of Ref. 15). The saddle-node itself emerges at $H_c = \pi$ from the dot at the origin (Fig. 4), then moves for increasing H towards larger norms and larger a^+. For $a^+ > a^+_{\mathrm{sn}}$ only the $n = 1/2^b$ branch exists.

V. STEADY STATES IN THE TWO-DIMENSIONAL CASE

All the 1D states obtained in Sec. IV (Fig. 4) correspond to laterally invariant 2D states, i.e., stratified layers $c_0(x, z) = c_0(z)$. They may be unstable with respect to lateral perturbations $c_1(z)\exp(\beta t + ikx)$ (cf. Sec. II C). Whenever a (real) eigenvalue β (growth rate) crosses zero we expect a branch of steady two-dimensional states to bifurcate from the stratified (or homogeneous) state. In the following, the results of the linear analysis are discussed alongside the bifurcation diagrams of the 2D states as obtained by the fully nonlinear analysis (cf. Sec. II B).

From the linear stability analysis of homogeneous films we deduct that the complexity of the bifurcation diagrams will increase with increasing film thickness and lateral domain size because an increasing number of modes becomes linearly unstable. Based on this we distinguish "thin films" ($0 < H < \pi$) where the homogeneous film is only unstable with respect to lateral modes, "medium films" ($\pi \leq H < 2\pi$) where additionally the first vertical structuring mode is unstable, and "thick films" ($2\pi \leq H$) where more vertical modes are unstable.

We distinguish four cases: flat and modulated films without and with energetic bias at the free surface. Each case is discussed for a number of thin and medium films of thicknesses $H < 2\pi$. Similar studies may be performed for thick films; however, then the bifurcation diagrams become rather crowded. In the cases with energetic bias we look at one to three different strengths a^+.

In each of these cases, we will determine several branches of steady solutions. To order the various solutions and to discuss relations between the branches, we employ some ideas from equivariant bifurcation theory.[38,42,43] This will allow us to infer the multiplicity of the various branches, the character of the symmetry breaking bifurcations and help to determine the stability of the solutions. Note, however, that we will sort our numerical results using a convenient selection of symmetries (reflections, inversions, and rotations in a space spanned by the spatial coordinates and the concentration). To keep the picture simple. we exclude whenever possible translations. A proper group theoretical treatment is beyond the scope of the present work.

A. Flat films without energetic bias

In the first case, we impose a flat free surface without energetic bias. This corresponds to the limit of large and concentration-independent surface tension. The symmetry group that leaves the system of equations, boundary, and integral conditions invariant is $\mathbf{Z}_2^x \times \mathbf{Z}_2^z \times \mathbf{Z}_2^c$ (cf. Ref. 44). The superscripts indicate which coordinate/field the symmetry refers to, i.e., $\mathbf{Z}_2^x \times \mathbf{Z}_2^z = \mathbf{D}_2^{xz}$ is the dihedral group of the rectangle that the domain forms in the (x, z)-plane and $\mathbf{Z}_2^c$ is a cyclic group of order 2 that corresponds to reflection in c, i.e., the transformation $c \to -c$. The corresponding

TABLE I. Group table for the symmetry group $\mathbf{D}_2^{xz}\times\mathbf{Z}_2 = \mathbf{Z}_2^x\times\mathbf{Z}_2^z\times\mathbf{Z}_2^c$ that leaves the system of equations, boundary, and integral conditions invariant for an imposed flat free surface without energetic bias. The σ_{ij} correspond to reflections at the plane spanned by the i and j axes, where i and j can take the values x, z, and c; the π_i are rotations by π about the i axis; and the ρ_{xzc} stands for an inversion.

	I	σ_{xz}	σ_{xc}	σ_{zc}	π_x	π_z	π_c	ρ_{xzc}
I	I	σ_{xz}	σ_{xc}	σ_{zc}	π_x	π_z	π_c	ρ_{xzc}
σ_{xz}	σ_{xz}	I	π_x	π_z	σ_{xc}	σ_{zc}	ρ_{xzc}	π_c
σ_{xc}	σ_{xc}	π_x	I	π_c	σ_{xz}	ρ_{xzc}	σ_{zc}	π_z
σ_{zc}	σ_{zc}	π_z	π_c	I	ρ_{xzc}	σ_{xz}	σ_{xc}	π_x
π_x	π_x	σ_{xc}	σ_{xz}	ρ_{xzc}	I	π_c	π_z	σ_{zc}
π_z	π_z	σ_{zc}	ρ_{xzc}	σ_{xz}	π_c	I	π_x	σ_{xc}
π_c	π_c	ρ_{xzc}	σ_{zc}	σ_{xc}	π_z	π_x	I	σ_{xz}
ρ_{xzc}	ρ_{xzc}	π_c	π_z	π_x	σ_{zc}	σ_{xc}	σ_{xz}	I

group table is given in Table I. The trivial homogeneous solution $c(x, z) = 0$ is invariant under the full group. All solutions that bifurcate from it must be invariant under one of its subgroups.

1. Thin film of thickness H = 2.5

For films of thickness $H = 2.5 < H_c = \pi$ layered or checker-board states do not exist (Sec. III). The trivial state is present for all domain sizes L and corresponds to the horizontal line at $||\delta c|| = 0$ ($E = 0.625$) in the bifurcation diagram in Fig. 6. For $L > L_c = \pi$, laterally structured films exist as expected from the linear analysis. The corresponding dispersion relation is given in Fig. 7 (case $a^+ = 0$). The growth rate β crosses zero at $k_c^{ls} = 1.0$, i.e., the critical domain size is $L_c^{ls} = 2\pi$.

In Fig. 6, the first four branches of laterally structured patterns are shown; with lateral mode numbers $s = 1/2, 1, 3/2$, and 2. We call them $(s, 0)$ branches, where the zero corresponds to the vertical mode number n. The first one bifurcates at $L = L_{1/2}^{ls} = \pi$ and consists of films laterally demixed into two parts. A typical concentration profile is given on the left of the second row of Fig. 8. The profiles on this $(1/2, 0)$ branch correspond to half a lateral period and are invariant under the subgroup $\{I, \sigma_{xc}, \pi_z, \rho_{xzc}\}$ and to translations $T_{L/s}^x = T_{2L}^x$, i.e., to translations in x by multiples of $2L$ in the embedded PBC system (see Ref. 44). The subgroup is the same for all branches where $2s$ is odd. The next branch bifurcates at $L = L_1^{ls} = 2\pi$. It is the first branch of periodic solutions and is therefore directly predicted by the linear stability analysis. The solutions consist of three different regions (see right hand profile of the second row of Fig. 8) and are invariant under the subgroup $\{I, \sigma_{xc}, \sigma_{zc}, \pi_c\}$

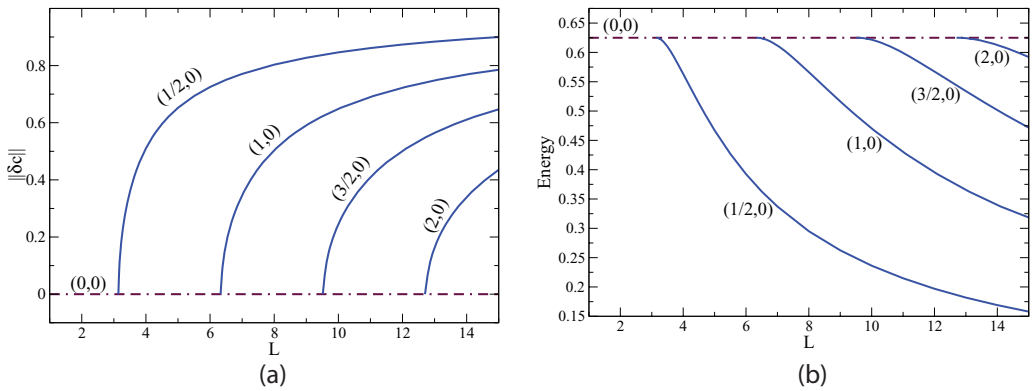

FIG. 6. The bifurcation diagram for steady state solutions in dependence of the domain size L for flat films of thickness $H = 2.5$, and without energetic bias ($a^+ = 0$). Shown are (a) the L_2-norm for the concentration field (Eq. (22)), and (b) the energy E (Eq. (24)). The dot-dashed horizontal line (maroon online) corresponds to the homogenous solution (0, 0) whereas the solid lines (blue online) are the various laterally structured film states $(s, 0)$.

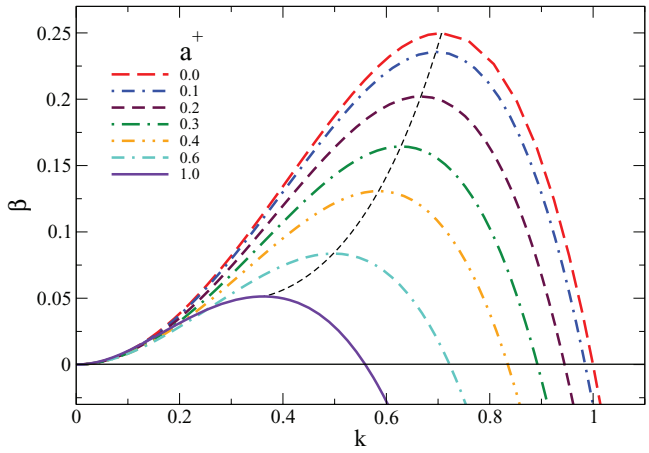

FIG. 7. The linear stability of a thin flat homogeneous film [(0, 0) branch for $H = 2.5$] is characterized by the dispersion relation, i.e., by the dependence of the growth rate on the lateral wave number. Shown are cases without ($a^+ = 0$) and with ($a^+ > 0$) energetic bias at the free surface for a^+ as given in the legend. Transport may occur via diffusion and convection, but the interface is kept flat. The thin dashed line (black online) is parameterized by a^+ and follows the maximum ($k_{\max}$, $\beta_{\max}$) of the dispersion relation.

and to translations $T^x_{L/s} = T^x_L$ by multiples of L in the PBC system. This applies to all branches with even $2s$. As the solutions have no vertical structure, all of them inherit the symmetry with respect to vertical reflection (σ_{xc}) from the trivial state. The corresponding relation of the subgroups together with example profiles are given in Fig. 8. Note that the bifurcations at the L^{ls}_s are actually pitchfork bifurcations. At each of them two branches emerge. Their solutions are related by the symmetry σ_{xz}: $c \to -c$. The importance of the various solutions in a real physical system may be deduced from their energies (Fig. 6(b)). For $L < \pi$ only the trivial state exists, and for $L > \pi$ the (1/2, 0) branch is always the one of lowest energy, i.e., the system will always evolve towards it. The other solutions might still occur as transient states during a lateral coarsening process.

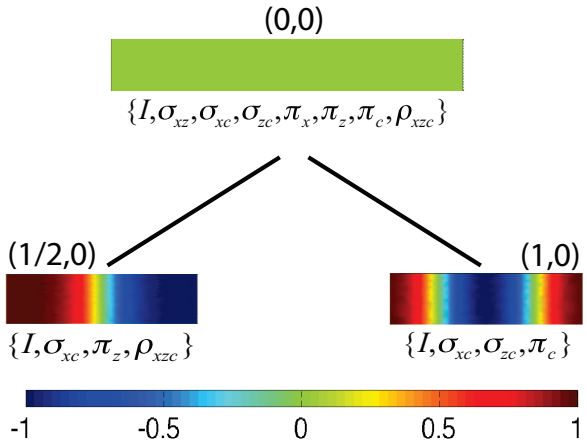

FIG. 8. For the case of films of thickness $H = 2.5$ without energetic bias, we show (i) typical steady concentration profiles on the (0,0), (1/2,0), and (1,0) branches, (ii) the corresponding symmetry groups and (iii) the subgroup relation between them that correspond to the pitchfork bifurcations in the bifurcation diagram of Fig. 6. Translations are not included in the scheme but are discussed in the main text. The concentration profiles for the (1/2, 0) and (1, 0) branch are at $L = 5$ and $L = 8$, respectively. The group table is given in Table I.

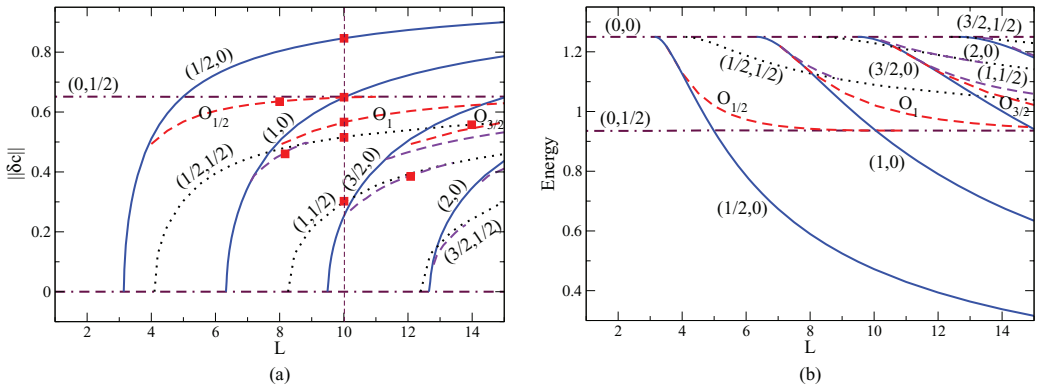

FIG. 9. The bifurcation diagrams for steady film solutions in dependence of the domain size L for flat films of thickness $H = 5$ and without energetic bias ($a^+ = 0$). Shown are (a) the L_2-norm for the concentration field, and (b) the energy E. The dot-dashed lines (maroon online) correspond to the laterally homogenous $(0, n)$-solutions for $n = 0$ (dash-dash-dot) and $n = 1/2$ (dash-dot); the solid lines (blue online) are laterally structured $(s, 0)$-states for $s = 1/2$, 1, 3/2, and 2; the dotted lines (black online) are checker-board $(s, 1/2)$-states for $s = 1/2$, 1, and 3/2; the dashed lines (red and purple online) corresponds to various types of oblique solutions that are further explained in the main text. The small squares (red online) in panel (a) mark solutions that are given in Fig. 10.

2. Film of medium thickness H = 5

In Sec. V A 1, we have studied films with $H < H_c = \pi$. There, no laterally homogeneous solutions exist beside the trivial one. For $H > H_c$ layered structures are possible. Here we consider $H = 5$, i.e., $H_c < H < 2H_c$, where the stratified bilayer (0, 1/2) branch exists but not the trilayer (0, 1) branch (cf. Fig. 4 at $a^+ = 0$). The corresponding bifurcation diagram is given in Fig. 9. For selected concentration profiles see Fig. 10. The horizontal lines in Fig. 9 represent the trivial (0, 0) branch ($||\delta c|| = 0$, $E = 1.25$) and the (0, 1/2) branch of two-layer stratified states ($||\delta c|| = 0.65$, E

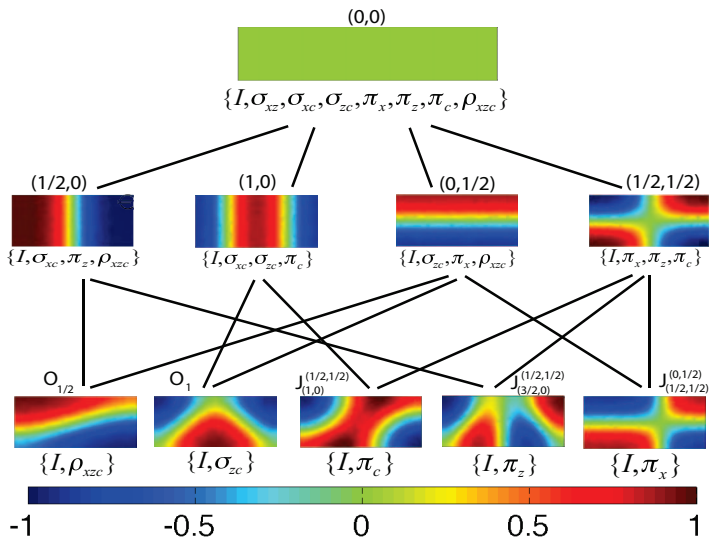

FIG. 10. For the case of films of thickness $H = 5$ without energetic bias, we show (i) typical steady concentration profiles on the various branches in the bifurcation diagram of Fig. 9, (ii) the corresponding symmetry groups, and (iii) the subgroup relations between them that correspond to the various occurring pitchfork bifurcations. Translations are not included in the scheme but are discussed in the main text. The concentration profiles on the second row are on branches (from the left): (1/2, 0), (1, 0), (0, 1/2), and (1/2, 1/2) all for $L = 10$, whereas the ones on the third row are on branches (from the left) $O_{1/2}$ at $L = 8$, O_1 at $L = 10$, $J^{(1/2,1/2)}_{(1,0)}$ that joins (1, 0) and (1/2, 1/2) at $L = 8.2$, $J^{(1,1/2)}_{(3/2,0)}$ joining (3/2, 0) and (1, 1/2) at $L = 12$, and $J^{(0,1/2)}_{(1/2,1/2)}$ that joins (1/2, 1/2) and (0, 1/2) at $L = 14$. They are marked by small squares in Fig. 9(a).

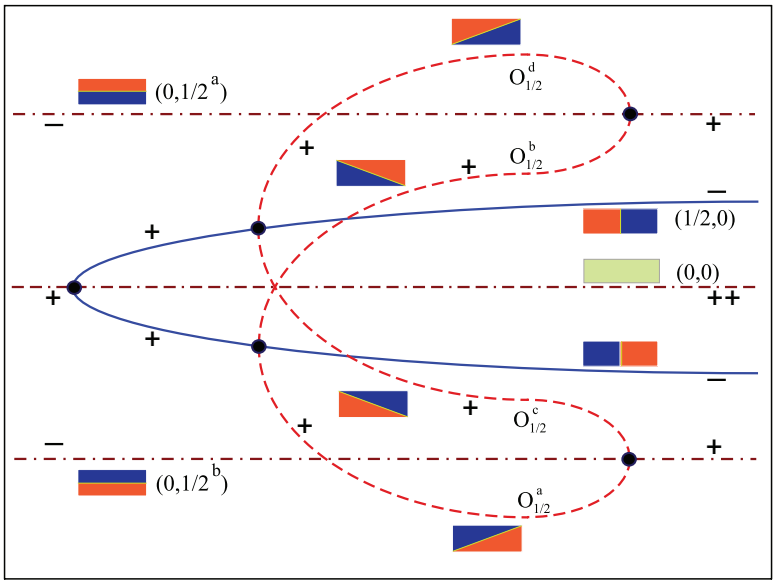

FIG. 11. Schematic bifurcation diagram for the various pitchfork bifurcations (marked by black dots) involved in the transitions between the (0, 0) branch of homogeneous films, the (1/2, 0) branches of laterally structured films, the $O_{1/2}$ branches of oblique solutions, and the (0, 1/2) branches of stratified films. The line styles correspond to the ones in Fig. 9. The symbols "+" and "−" indicate the stability of the branches, and the small pictograms indicate the various decomposition patterns on the branches [Lighter gray: liquid 1 (red online)] and [darker gray: liquid 2 (blue online)].

$= 0.94$) [see 3rd profile on the middle row in Fig. 10]. Again there are two (0, 1/2) branches with the same global measures whose solutions are related by the symmetry σ_{xz}: $c \to -c$.

They correspond to half a vertical period and are invariant under the subgroup $\{I, \sigma_{zc}, \pi_x, \rho_{xzc}\}$ and under translations $T^z_{H/n} = T^z_{2H}$ in z by multiples of $2H$ in the PBC system. The (0, 1) branch exists only at larger $H > 2\pi$ and has solutions that correspond to trilayer or sandwich films. They are invariant under the subgroup $\{I, \sigma_{zc}, \sigma_{xc}, \pi_c\}$ and under translations $T^z_{H/n} = T^z_H$ in z by multiples of H in the PBC system. We will not discuss them further and do not include them or the related secondary branches in Fig. 10.

As for $H = 2.5$, the branches of laterally structured films bifurcate from the trivial one at $L^{ls}_s = 2s\pi$. Figure 9 gives the branches with the lateral mode numbers $s = 1/2$, 1, 3/2, and 2. Concentration profiles are shown for $s = 1/2$ and $s = 1$ on the second row of Fig. 10. Comparing Figs. 9 and 6, one notices that for all branches with $n = 0$, the energy in the $H = 5$ case is twice the one for $H = 2.5$. The norms for the concentration fields are identical. This is as expected for the present case without energetic bias.

The two laterally structured (1/2, 0) branches are linearly unstable when they emerge from the (0, 0) branch at $L = \pi$, then they stabilize at symmetry-breaking pitchfork bifurcations at about $L = 3.9$ where four branches of oblique solutions ($O_{1/2}$) emerge (two from each (1/2, 0) branch). A profile is given on the very left of the third row of Fig. 10. The four branches end at about $L = 11.0$ in two further pitchfork bifurcations on the (0, 1/2) branches (Fig. 9). The schematic bifurcation diagram in Fig. 11 illustrates the multiple branches. For each branch it also indicates the stability and provides a pictogram of the corresponding decomposition pattern. Along the oblique branches, the originally [on (1/2, 0) branches] vertical liquid-liquid interface turns until it becomes horizontal [on (0, 1/2) branches]. Note that both the (1/2, 0) and the (0, 1/2) branches are linearly stable for $3.9 < L < 11.0$, i.e., where the $O_{1/2}$ branches exist. All the solutions on all the $O_{1/2}$ branches are invariant under the subgroup $\{I, \rho_{xzc}\}$ and under translations T^x_{2L} by multiples of $2L$ in the PBC system. The corresponding relations between the mentioned subgroups are given in Fig. 10.

Similar sets of branches of oblique solutions connect all $(s, 0)$ branches with the (0, 1/2) branch. We call them O_s branches. A profile on the O_1 branch that connects the (1, 0) and the (0, 1/2) branch is given in Fig. 10 (second on row three). Other branches of oblique solutions connect checker-board

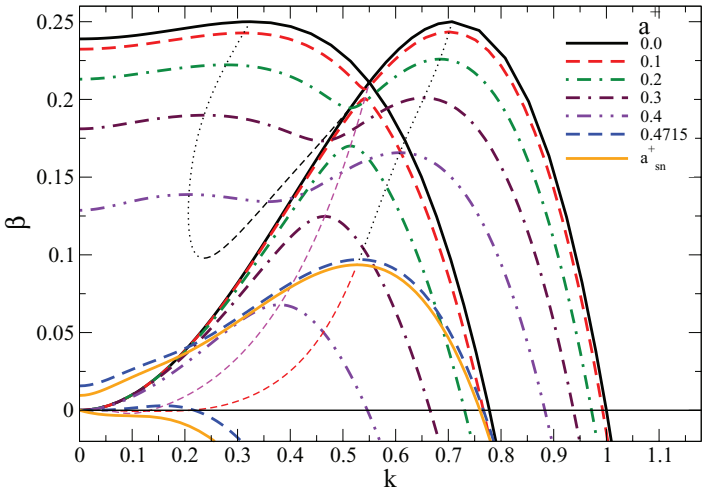

FIG. 12. The linear stability of a flat homogeneous film of medium thickness [(0, 0) branch for $H = 5.0$] is characterized by the dispersion relation. Shown are the cases without ($a^+ = 0$) and with ($a^+ > 0$) energetic bias at the free surface for a^+ as given in the legend. Given are two sets of dispersion curves: for the lateral instability mode (larger $k_{\max}$ at $a^+ = 0$), and for the checker-board instability mode (smaller $k_{\max}$ at $a^+ = 0$). The thin dotted and dashed lines (black, magenta, and red online) are parameterized by a^+ and follow the maxima ($k_{\max}$, $\beta_{\max}$) and minima of the dispersion relations.

branches (discussed next) and various (s, 0) branches. Figure 9 shows in total eight branches of oblique solutions.

Another type of solution that becomes possible for $H > H_c$ are checker-board states. They bifurcate from the homogeneous solution at $L^{\mathrm{cb}}_{s,n} = sL^{\mathrm{cb}}_n$ [cf. Fig. 3 and Eq. (29)]. For $H = 5$, we only have states with $n = 1/2$, giving $L^{\mathrm{cb}}_{1/2} = 10\pi/\sqrt{25 - \pi^2} = 8.08$ (see also the leftmost dispersion curve in Fig. 12 that crosses zero at $k_c = 0.78$, i.e., results in a critical L of 8.06). The first checker-board branch is denoted by (1/2, 1/2) and emerges at $L^{\mathrm{cb}}_{1/2,1/2} = 4.04$ (see Fig. 9 and rightmost concentration profile on second row of Fig. 10). Note that the values obtained with the different methods do well agree. The (1/2, 1/2) states are invariant under the subgroup $\{I, \pi_x, \pi_z, \pi_c\}$ and under translations T^x_{2L} by multiples of $2L$ and T^z_{2L} by multiples of $2H$ in the PBC system. Their branch is connected to the (s, 0) branches (with $s > 1/2$) via branches of oblique solutions (two profiles are given on row three of Fig. 10) that are all invariant under $\{I, \pi_c\}$ (branches $J^{(1/2,1/2)}_{(1,0)}$ and $J^{(3/2,1/2)}_{(2,0)}$) or $\{I, \pi_z\}$ (branch $J^{(1/2,1/2)}_{(3/2,0)}$) or $\{I, \rho_{xzc}\}$ (branch $J^{(1,1/2)}_{(3/2,0)}$). The checker-board branch is also connected to the layered (0, 1/2) branch. The connecting $J^{(0,1/2)}_{(1/2,1/2)}$ branch is invariant under $\{I, \pi_x\}$ (see e.g., the rightmost profile on row three of Fig. 10). All the ones mentioned are invariant under translations T^x_{2L} and T^z_{2L} in the PBC system. The relations between subgroups corresponding to the various steady states for such films are given in Fig. 10. Note that all the discussed branches emerge via pitchfork bifurcations. At each such bifurcation there emerge two branches that are related by the symmetry that is broken. The schematic bifurcation diagram in Fig. 13 illustrates this for the secondary branches emerging from the (1/2, 1/2) and (1, 0) branches. For each branch it also indicates the stability and provides a pictogram of the corresponding decomposition pattern.

Due to the existence of vertical and horizontal liquid-liquid interfaces, the checker-board solutions have a rather large energy. Note that all liquid-liquid interfaces of the checker-board and laterally structured solutions meet the free surface at an angle of $\pi/2$ corresponding to the zero energetic bias ($a^+ = 0$). An exception are the oblique solutions where two liquid-liquid interfaces meet the free surface at the same point. This allows for an angle of $\pi/4$ (see Fig. 10, second profile on row three).

Finally, we discuss the importance of the various solutions in a physical system based on their energies (Fig. 9(b)). In contrast to the case of $H = 2.5$, here the trivial state is always unstable: below $L^{ls}_c = \pi$ with respect to the vertical $n = 1/2$ instability mode and above L^{ls}_c additionally to the lateral $s = 1/2$ instability mode. Both, the stratified (0, 1/2) branch and the laterally structured (1/2, 0)

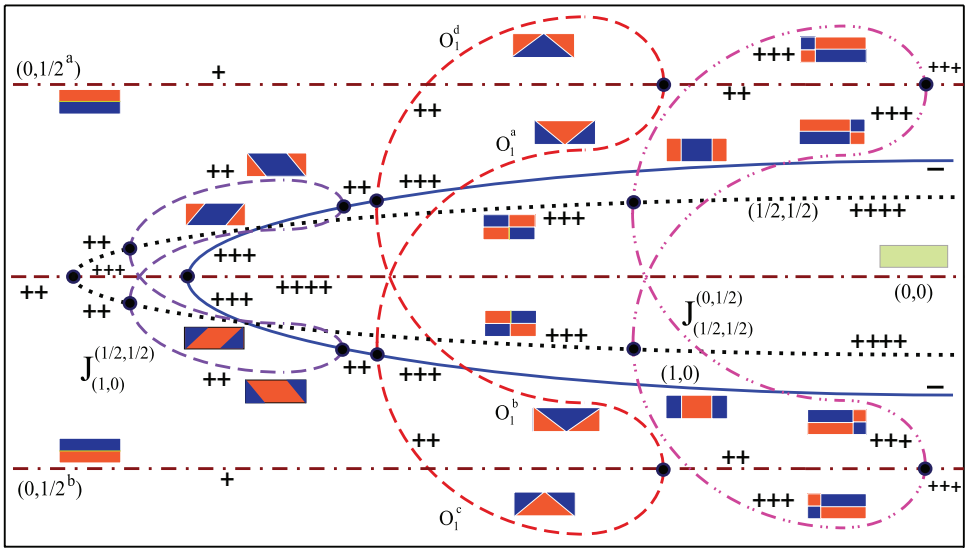

FIG. 13. Schematic bifurcation diagram for the various pitchfork bifurcations (marked by black dots) involved in the transitions between the (0, 0) branch of homogeneous solutions, the (1, 0) branches of laterally structured states, the (1/2, 1/2) branches of checkerboard state, the O_1 branches of oblique solutions, and the (0, 1/2) branches of stratified states. The line styles correspond to the ones in Fig. 9. The symbols "+" and "−" indicate the stability of the branches, and the small pictograms indicate the various decomposition patterns on the branches [lighter gray: liquid 1 (red online)] and [darker gray: liquid 2 (blue online)].

branch are linearly stable between the pitchfork bifurcations that limit the range of existence of the $O_{1/2}$ branch. The latter consists of unstable threshold solutions that have to be overcome to switch between the two stable branches. Note that the Maxwell point L_{maxw} where the (1/2, 0) branch and the (0, 1/2) branch are of equal energy lies well inside the interval. An estimate determined in the limit of a sharp liquid-liquid interface gives $L_{\mathrm{maxw}} = H/(1 - a^+) = 5$, actually, a trivial result for $a^+ = 0$. All other solutions are of higher energy and might only occur as transient states during a coarsening process. They might also gain importance for ratios S of interfacial tensions that are larger than one.

B. Flat films with energetic bias

Next, we study films with a linear energetic bias ($a^+ > 0$) at the flat free surface. The homogeneous state $||\delta c|| = 0$ only exists in the neutral case ($a^+ = 0$). When increasing a^+, the film becomes weakly stratified. The norm $||\delta c||$ increases, whereas the energy slightly decreases (cf. Figs. 4 and 5 above). Note that the energetic bias breaks the σ_{xz}: $c \to -c$ symmetry. In consequence, the symmetry group under which the equations and boundary conditions are invariant is smaller than the one for the system without bias. It corresponds to $\mathbf{Z}_2^x$ (with elements $\{I, \sigma_{zc}\}$) and the translations T_∞^x (see Ref. 44). The bias also results in an increasing distinction between many of the profiles that had in the case without bias emerged in a common pitchfork bifurcation. In the case of the two-layer stratified films this is well visible in Figs. 4 and 5. Now, the solution with component 2 at the free surface is energetically preferred. The second stratified solution (fluid 1 at the free surface) annihilates with the weakly stratified state in a saddle node bifurcation at a^+_{sn} (Fig. 4).

1. Thin film of thickness H = 2.5

As the bifurcation diagram for biased flat films with $H = 2.5$ looks rather similar to the one for the neutral case (Fig. 6), we only mention the important differences: (i) The weakly stratified branch takes the role of the trivial homogeneous branch in the neutral case. The corresponding profiles are invariant under $\{I, \sigma_{zc}\}$ and translations T_∞^x; (ii) The points L_s^{ls} where the laterally structured

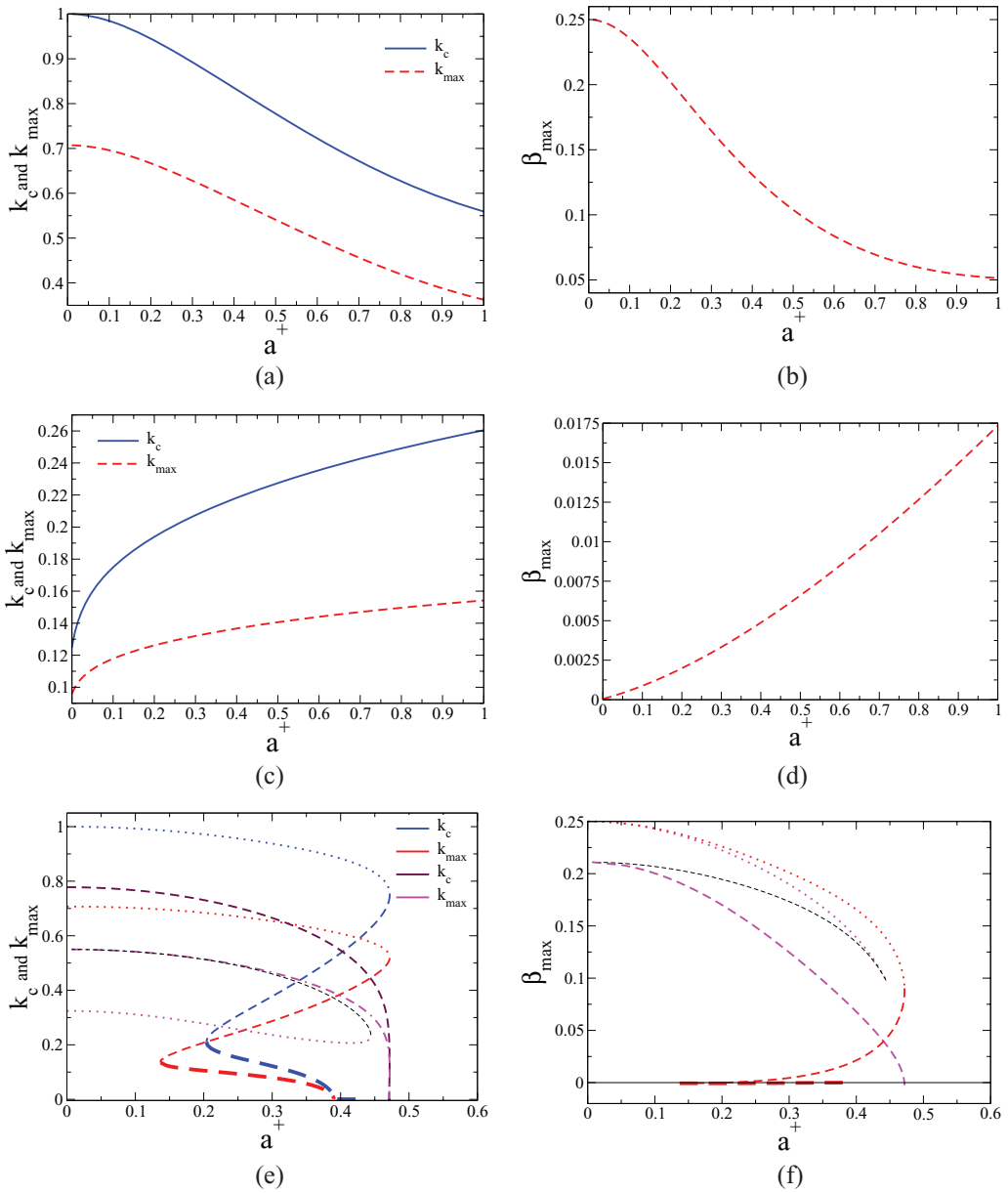

FIG. 14. Characteristics of the dispersion relations are given as functions of the energetic bias a^+ at the flat free surface for (a,b) homogeneous films of $H = 2.5$, (c,d) the $(0, 1/2^b)$ branch for $H = 5$, and (e,f) the $(0, 0)$, $(0, 1/2^a)$ branches for $H = 5$ (cf. Figs. 4, 7, 12, and 17). The left column gives the critical wavenumber k_c (for line styles see legend) and the wave number of the fastest growing mode $\mathbf{k}_{\max}$ while the right column gives the corresponding maximal growth rate $\beta_{\max}$ (with the linestyles corresponding to the ones of $k_{\max}$). The situation in the last row is involved as (i) two branches join in the saddle node at $a^+_{\text{sn}} \approx 0.47$ and (ii) there are two unstable modes that can have maxima and minima at $k \neq 0$ [cf. Figs. 12 and 17(b)]. The lines in (e,f) show the loci of maxima and minima employing the same linestyles as used to track them in Fig. 12. In particular, the additional dashed (brown online) and dash-dash-dotted (magenta online) line give k_c and $k_{\max}$ for the checkerboard mode. For further discussion see main text.

branches bifurcate shift to larger L as a^+ is increased, corresponding to a decreasing critical wave number k_c (Fig. 14). Laterally structured solutions are only invariant under translations $T^x_{L/s}$ and the identity $\{I\}$ ($2s$ odd) or $\{I, \sigma_{zc}\}$ ($2s$ even); (iii) The angle between the diffuse liquid-liquid interface and the liquid-gas interface is not $\pi/2$ anymore as the preferred fluid 2 now occupies a larger part of the free surface than fluid 1. Therefore, the notion "laterally structured film" is not literally correct

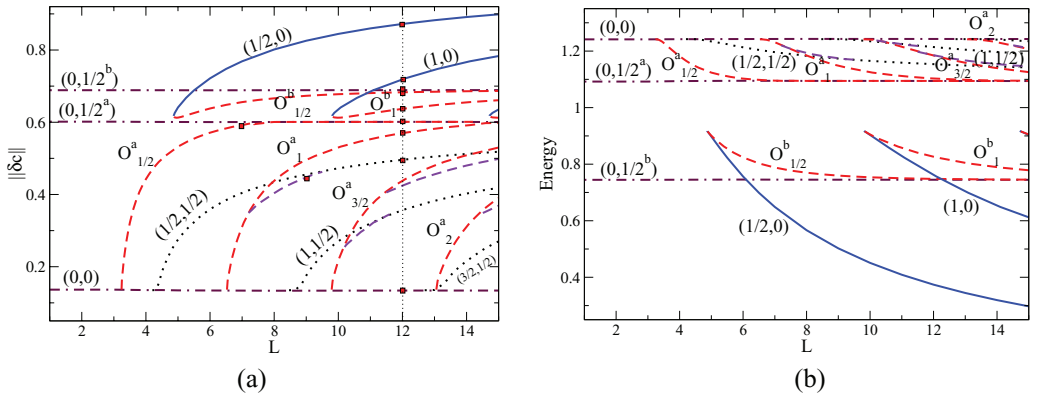

FIG. 15. Bifurcation diagrams for steady state solutions in dependence of the lateral domain size L, for flat films of thickness $H = 5$ with a moderate energetic bias at the free surface ($a^+ = 0.2$). Panels (a) and (b) give the L_2-norm of the concentration field and the energy, respectively. The dash-dash-dotted line (maroon online) represents the trivial (weakly stratified) solution, the dash-dotted (maroon online) lines represent the stratified (0, $1/2^a$) and (0, $1/2^b$) branches, the solid curves (blue online) represent the laterally structured (s, 0) branches ($s = 1/2$, 1), the dashed lines (red online) represent the oblique branches O_s^a ($s = 1/2$, 1, 3/2, 2) and O_s^b, $s = 1/2$, 1, and the dotted curves (black online) represent the checker-board (s, 1/2) branches ($s = 1/2$, 1, 3/2).

anymore. However, we continue to use it as it indicates to which solution at $a^+ = 0$ the solution at hand is related. (iv) For rather high $a^+ \approx 1$, the bifurcation from the trivial state is subcritical and there exist (even for $H < \pi$) solutions with an oblique liquid-liquid interface that represent a transition state between the weakly stratified and laterally structured branches. The branch of oblique solutions joins the laterally structured film in a saddle node bifurcation when the diffuse interface passes the corners of the domain.

The linear stability of the stratified states is analyzed for several $a^+ > 0$ in Fig. 7 above. The maximal growth rate $\beta_{\max}$ and the critical wavenumber k_c are given as functions of a^+ in Figs. 14(a) and 14(b), respectively. At $a^+ = 0$, one has $k_c = 1$ and $\beta_{\max} = 0.25$. Both decrease as a^+ increases. Overall the bias makes the films less unstable, and correspondingly the bifurcation points $L_s^{ls} = 2s\pi/k_c$ are shifted towards larger domain sizes. Next we consider thicker films with $H = 5 > \pi$.

2. Film of medium thickness H = 5

Increasing a^+ from zero for flat films of thickness $H = 5$ results in significant changes in the bifurcation diagrams. Consider, e.g., the points on the line $a^+ = 0.2$ in Fig. 4. The two stratified solution branches (0, $1/2^a$) and (0, $1/2^b$) now differ resulting from the broken symmetry σ_{xz}: $c \to -c$. In consequence, the related (four-fold) oblique branch O_s (cf. Fig. 9) splits into 2 two-fold branches. The solutions on the two that form each pair are related by σ_{zc}: $x \to -x$. For the resulting bifurcation diagram see Fig. 15. The split oblique solutions branches are called O_s^a and O_s^b and are given as dashed lines (red online). One of them now ends in a (symmetry-conserving) saddle-node bifurcation together with the laterally structured branch. The other one continues towards the weakly stratified solution. Corresponding profiles, their symmetry groups and relations between them are given in Fig. 16. The checker-board solutions do not split with increasing a^+ because both branches behave identically (they are related by the translation $T^x_{L/2s}$). The oblique branches O_s^a approach the stratified (0, $1/2^a$) branch but do actually not bifurcate from it in the L-range given in Fig. 15. The oblique branches O_s^b bifurcate from the stratified (0,$1/2^b$) branch in good agreement with the linear results of Fig. 17.

A similar split occurs for all the J branches (that connect the various checkerboard branches to other branches). For $a^+ = 0$ they are four-fold (cf. Fig. 13), but for $a^+ > 0$ each splits into two two-fold branches. However, the resulting difference between the branches is very small and not well visible in Fig. 15. In consequence, the connection between the J branches and the checkerboard

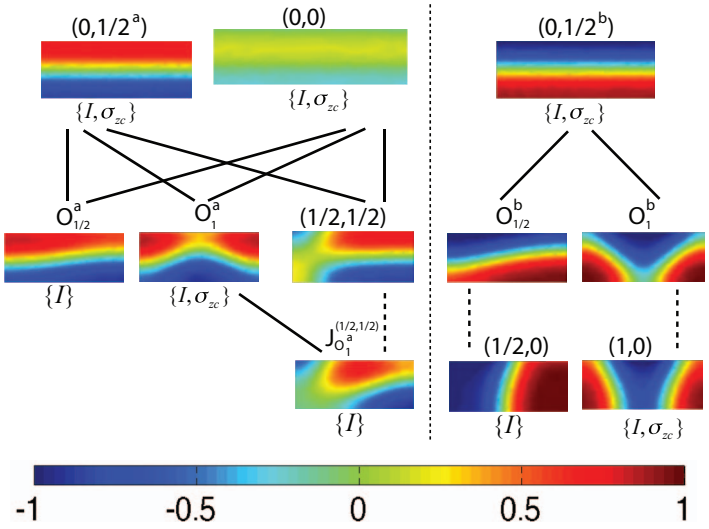

FIG. 16. For the case of films of thickness $H = 5$ with energetic bias, we show (i) typical steady concentration profiles on the various branches in the bifurcation diagram of Fig. 15, (ii) corresponding symmetries and (iii) the relations between the branches that correspond to the various symmetry-breaking pitchfork and not symmetry-breaking saddle-node bifurcations as solid and dashed straight lines, respectively. Symmetries with respect to translations are not included in this and similar schemes throughout the paper but are discussed in the main text when relevant. Here, in two of the pitchfork bifurcation from the laterally invariant (0, 0) and (0, 1/2) solutions, the translational symmetry T^x_∞ is actually the only one that is broken. The concentration profiles on the first row are on branches (from the left): (0, $1/2^a$), (0, 0), and (0, $1/2^b$) all for $L = 12$, whereas the ones on the second row are on branches (from the left) $O^a_{1/2}$ at $L = 7$, O^a_1 at $L = 12$, (1/2, 1/2) at $L = 12$, $O^b_{1/2}$ at $L = 12$, O^b_1 at $L = 12$, the ones on the third row are on branches (from the left) $J^{(1/2,1/2)}_{O^a_1}$ that joins O^a_1 and (1/2, 1/2) taken at $L = 9$, (1/2, 0), and (1, 0) both at $L = 12$. The vertical dotted line separates solutions on the high (left) and low (right) energy group of branches (see main text).

branches is not a pitchfork bifurcation anymore: It is replaced by a saddle node bifurcation between the left hand part of the checkerboard branches and one of the two-fold J branches and a continuous transition between the other two-fold J branch and the right hand part of the checkerboard branch. This agrees with the fact that the J branches and the checkerboard branches they connect to, have the same symmetry (see Fig. 16).

In general, one may distinguish a high and a low energy group of solution branches (Fig. 15(b)). The high energy group consists of the weakly stratified (0, 0), the stratified (0,$1/2^a$), all checkerboard (s, 1/2), and all oblique O^a_s and J branches (see profiles left of dotted line in Fig. 16). All of them are confined between the (0, 0) and (0, $1/2^a$) branch. Figure 4 shows that an increase in the bias a^+ increases the difference between the stratified (0, $1/2^a$) and (0, $1/2^b$) branches. However, the difference between the (0, 0) and (0, $1/2^a$) branch decreases. They approach each other and annihilate at the saddle-node at $a^+_{\rm sn}$. In consequence, the entire group of high energy solutions vanishes at $a^+_{\rm sn}$. Only the low energy group remains for $a > a^+_{\rm sn}$. It consists of the stratified (0,$1/2^b$) branch, the laterally structured (s, 0) branches, and the oblique O^b_s branches that connect the other two (see profiles right of dotted line in Fig. 16).

Next we consider how well the primary bifurcations in Fig. 15 agree with the linear stability results. Nearly all stratified solutions become unstable to lateral perturbations above some critical L_c (as discussed for $a^+ = 0$). Figure 12 above gives the dispersion relations for the weakly stratified film for various a^+. Figures 14(c) and 14(d) show as dotted lines k_c, $k_{\rm max}$ and $\beta_{\rm max}$ as a function of a^+. The two respective dispersion relations for each a^+ correspond to checker-board and lateral mode, respectively. For $a^+ = 0.2$, the growth rates cross zero (Fig. 12) at about $k_c \approx 0.73$, i.e., $L^{cb}_1 = 8.6$ (checker-board mode), and at $k_c \approx 0.97$, i.e., $L^{ls}_1 = 6.5$ (lateral mode). This agrees well with the values for the $s = 1$ branches in the bifurcation diagram of Fig. 15.

Figure 17 gives dispersion relations for the two stratified (0, 1/2) branches, whereas Figs. 14(c)–14(f) give k_c, $k_{\rm max}$ and $\beta_{\rm max}$ for the two branches as thick solid and dashed lines,

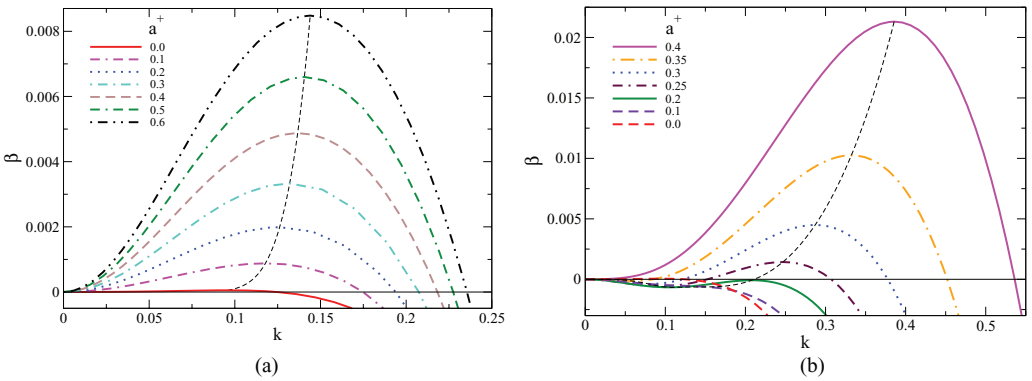

FIG. 17. Linear stability with respect to lateral perturbations for the stratified (a) $(0, 1/2^b)$ and (b) $(0, 1/2^a)$ branch at $H = 5$ for various biases a^+ as given in the legend. The thin dashed lines (black online) are parameterized by a^+ and follow the maxima $(k_{\max}, \beta_{\max})$ of the dispersion relations.

respectively. The behaviour of the energetically favourable $(0, 1/2^b)$ branch is straightforward [Fig. 17(a) and Figs. 14(c) and 14(d)]: The larger the bias the more unstable with respect to lateral perturbations it becomes. Critical and fastest growing wavenumber and maximal growth rate all increase with a^+. At $a^+ = 0.2$, we find $k_c = 0.19$, i.e., $L_c = 33.1$. This agrees well with the point where the $O^b_{1/2}$ bifurcates from the stratified $(0, 1/2^b)$ branch a bit above $L = 16$ (slightly beyond the right hand border of Fig. 15).

The situation is more intricate for the $(0, 1/2^a)$ branch [see Fig. 17(b) and Figs. 14(e) and 14(f)]. When increasing a^+, first the critical wavenumber and maximal growth rate decrease, the solution becomes stable against lateral perturbations at about $a^+ \approx 0.05$. Note that this part is not visible in Figs. 14(e) and 14(f) as growth rate and wavenumber are very small. However, a further increase in a^+ leads to a finite wavelength instability slightly above $a^+ = 0.2$ with $k_c \approx 0.21$ [see Fig. 17(b), curve for $a^+ = 0.2$ and folds in Figs. 14(e) and 14(f)]. Therefore, at $a^+ > 0.2$, there should be two more bifurcations of solutions of period one at about $L_c \approx 30$. In Fig. 15, it seems that the $O^a_{1/2}$ branch bifurcates from the $(0, 1/2^a)$ branch at about $L = 7.5$. This is, however, not the case. Upon inspection, the respective solutions on the two branches look still rather different implying that the $O^a_{1/2}$ branch continues to exist for larger L. Our linear stability results actually indicate that it exists for arbitrary large L as the $(0, 1/2^a)$ branch is linearly stable. However, as the bifurcations come into being at slightly larger a^+, our numerical procedure is not able to capture the $O^a_{1/2}$ branch at larger L. At larger a^+, the $(0, 1/2^a)$ solution is only unstable with respect to the related lateral mode in a range of wave numbers. For instance, at $a^+ = 0.3$, the $(0, 1/2^a)$ film is unstable between $k = 0.125$ and $k = 0.357$ (see Fig. 17(b)). The band of unstable wave numbers widens till the smaller one reaches zero (cf. curve for $a^+ = 0.4$ in Fig. 17(b) and k_c in Fig. 14(c)). Here, we will not discuss these effects further.

Finally, we briefly discuss the behaviour for $a^+ > a^+_{\text{sn}}$. Slightly above a^+_{sn}, the low energy group of branches does not change its appearance. At large a^+, however, additional structures appear, see the bifurcation diagram in Fig. 18 for an example ($a^+ = 0.8$). Although the laterally structured (1/2, 0) solutions ultimately still annihilate at low L with the oblique $O^b_{1/2}$ branch, the branch has acquired an additional pair of saddle node bifurcations, i.e., in a small range in L there exist now three stable and two unstable profiles. Further details are discussed in Ref. 35.

C. Height-modulated films without energetic bias

Now we lift the restriction of an imposed flat free surface and study films with a surface that is free to move. Practically, this is done by reducing the value of α to 1 in Eq. (7). In consequence, solutions are then not only characterized by the energy E and norm $||\delta c||$ of the concentration field, but also by the norm $||\delta h||$ of the film thickness profile $h(x)$ [see Eq. (23)]. We start with an investigation of the behaviour without energetic bias at the free surface ($a^+ = 0$) for films with $H = 2.5$ and $H = 5$. The case $a^+ > 0$ is briefly treated in Sec. V D. The main difference to the case

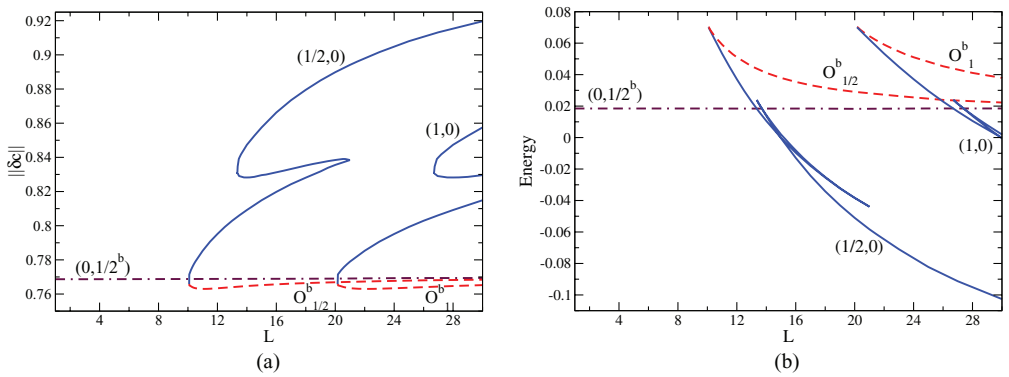

FIG. 18. Bifurcation diagram for steady state solutions for flat films of thickness $H = 5$ with a free surface with a large energetic bias of $a^+ = 0.8$. Given (a) the L_2-norm of the concentration field and (b) the energy as functions of the lateral domain size L. The dot-dashed horizontal line (maroon online) corresponds to the (0, 0) branch, the solid lines (blue online) are the laterally structured (s, 0) branches and the dashed lines (red online) correspond to the oblique solutions.

of an imposed flat surface is that now the free surface reacts to non-homogeneous concentration profiles. In the contact region of a diffuse interface between the two components and the free surface the horizontal and vertical force components have to be balanced. On the one hand, this leads to changes in all solutions discussed above in the case of a flat surface. On the other hand, it allows for new solutions that only exist because of the new degree of freedom.

To illustrate the changes in the known solutions, we show in Fig. 19 a film from the (1/2, 0) branch. The concentration profile shows lateral structuring, the liquid-liquid interface is still vertical, and $\theta \equiv \theta_1 = \theta_2 = 2\pi/3$, where θ_i is the angle between the liquid-liquid interface and the free surface of liquid i. In the sharp interface limit $\cos(\pi - \theta) = 1/(2S)$ (see Sec. II A).

1. Films of small thickness (H = 2.5)

For $H = 2.5$, the bifurcation diagram in terms of $||\delta c||$ (see Fig. 20(a)) looks rather similar to the one for flat films (Fig. 6(a)). As expected, the points L_s^{ls} where the laterally structured branches bifurcate are identical to the ones in the flat case; however, the $||\delta c||$ along the bifurcating branch is slightly larger than in the flat case (at max ≈5% for the parameter values we study). The energy is lower than in the flat case (not shown) mainly resulting from the additional degree of freedom that can be appreciated in Fig. 6(b) where $||\delta h||$ is shown. On every laterally structured branch (s, 0), the surface modulation monotonically increases with the lateral domain size. Typical profiles, their symmetries, and the relations between them are given in Fig. 21. The dispersion relation for

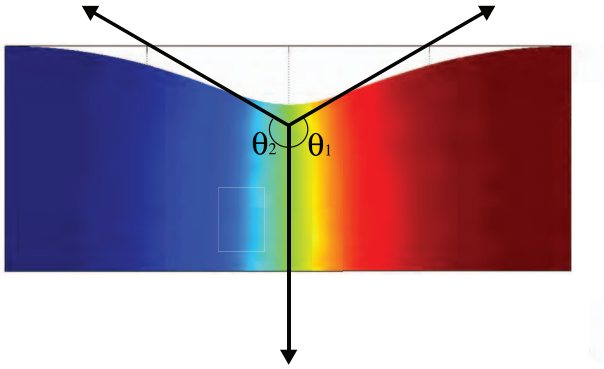

FIG. 19. Typical profile of a laterally phase-separated film with a modulated free surface without energetic bias ($a^+ = 0$). Shown is the profile at $L = 8$ from the (1/2, 0) branch for $H = 2.5$. The arrows indicate the forces on the contact region where the diffuse liquid-liquid and the sharp free surface meet.

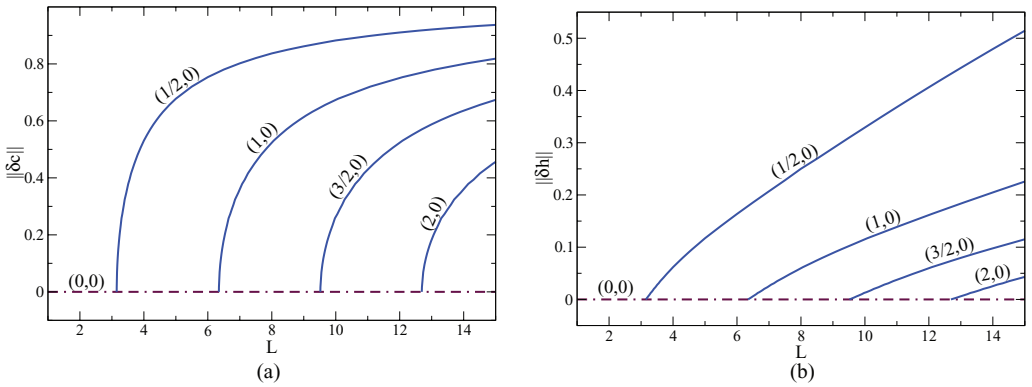

FIG. 20. The bifurcation diagram for steady state solutions in dependence of the domain size L for films with surface modulations of thickness $H = 2.5$, and without energetic bias ($a^+ = 0$). Shown are (a) the L_2-norm for the concentration field Eq. (22), and (b) the L_2-norm for the surface modulations Eq. (23). The dot-dashed horizontal line (maroon online) corresponds to the homogenous solution (0, 0) whereas the solid lines (blue online) are the various laterally structured film states.

the homogeneous solutions is given below in Fig. 22 (case $a^+ = 0$) and is identical to the one in the case of a flat surface (cf. Fig. 7).

Note that the symmetry group for the homogeneous solution is identical to the one in the flat non-biased case, whereas the ones of the laterally structured branches do not agree (cf. Fig. 8). This is due to the fact that any lateral structuring causes a surface modulation and therefore also breaks the $z \to -z$ symmetry. For fixed domain size, the branches of higher mode number have a smaller surface modulation as more diffuse interfaces "pin" the free surface.

2. Films of medium thickness ($H = 5.0$)

Increasing the film height to $H > \pi$ layered solutions become possible, a situation analyzed for neutral and biased flat films in Sec. V B. Allowing the free surface to change its profile, on the one hand modifies the already known solutions. On the other hand, we find that a modulated surface allows for additional large-amplitude solutions.

The bifurcation diagram for $H = 5.0$ for films of unbiased modulated surface is given in Fig. 23. A selection of corresponding profiles, their symmetry groups and relations between them are given in Fig. 24. Inspecting Figs. 23(a) and 23(b), i.e., the bifurcation diagrams in terms of $||\delta c||$ and E,

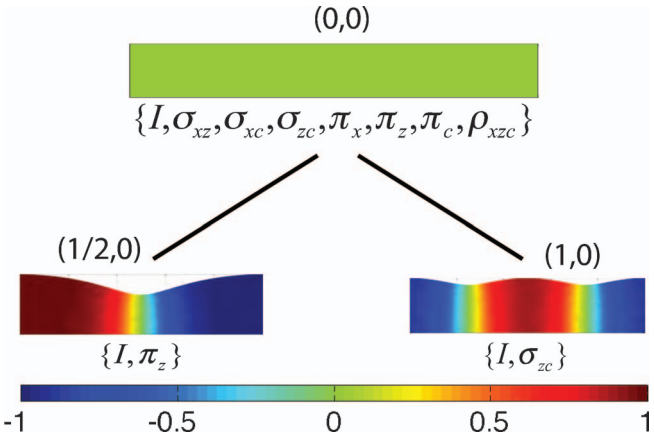

FIG. 21. For the case of height modulated films of thickness $H = 2.5$ without energetic bias, we show (i) typical steady concentration profiles on the (0,0), (1/2,0) and (1,0) branches, (ii) the corresponding symmetries and (iii) the relations between the branches (cf. bifurcation diagram Fig. 20). The concentration profiles for the (1/2, 0) and (1, 0) branch are at $L = 10$. For remarks on symmetries and line styles, see caption of Fig. 16.

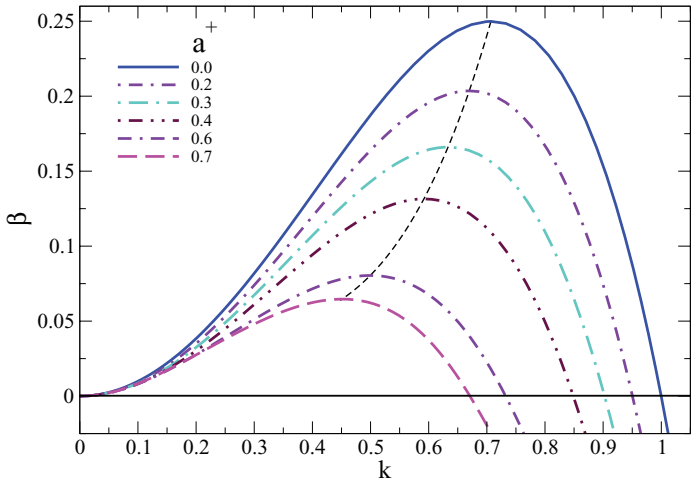

FIG. 22. Linear stability for thin films ($H = 2.5$) with modulated free surface ($\alpha = 1$). The dispersion relation is shown for different energetic biases at the free surface (see legend) for the homogeneous (weakly stratified) branch (0, 0) as a function of the wave-number k. The thin dashed line (black online) is parameterized by a^+ and follows the maximum ($k_{\max}$, $\beta_{\max}$) of the dispersion relation.

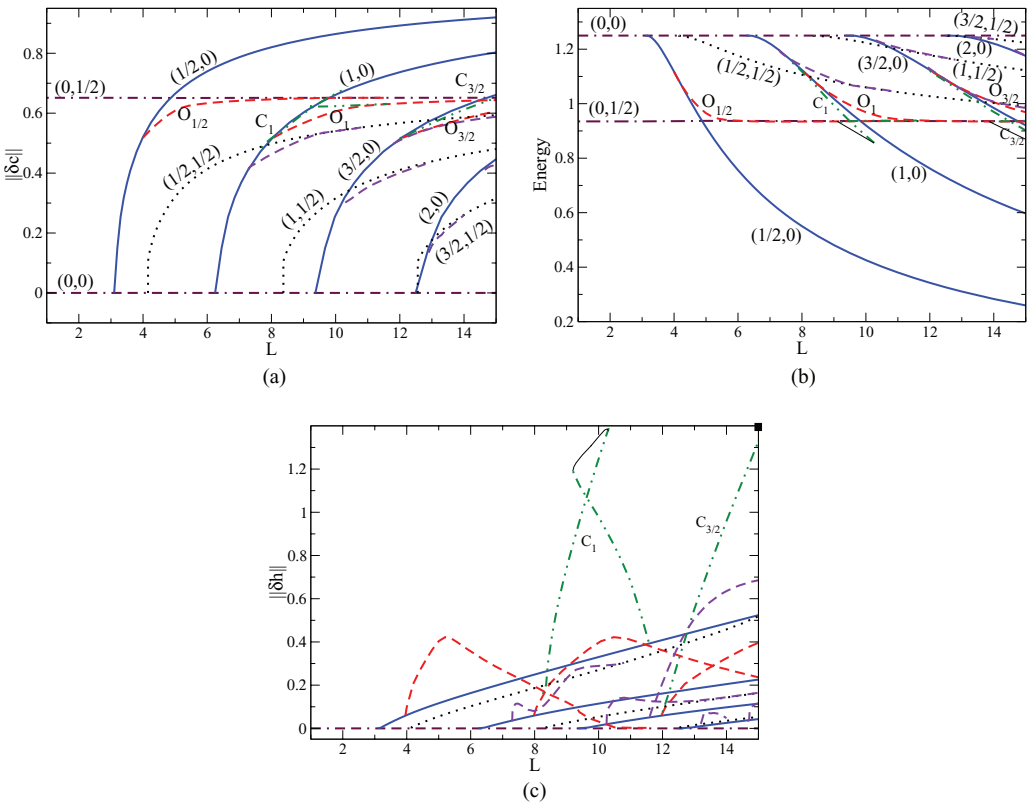

FIG. 23. The bifurcation diagrams for steady film solutions in dependence of the domain size L for modulated films of thickness $H = 5$ and without energetic bias ($a^+ = 0$). Shown are (a) the norm $||\delta c||$, (b) the energy E, and (c) the norm $||\delta h||$. The dot-dashed horizontal lines (maroon online) correspond to the laterally homogenous (0, n) solutions for $n = 0$ (dash-dash-dot) and $n = 1/2$ (dash-dot); the solid lines (blue online) are laterally structured (s, 0) states for $s = 1/2$, 1, 3/2, and 2; the dotted lines (black online) are checker-board (s, 1/2) states for $s = 1/2$, 1 and 3/2; the dashed lines (red and purple online) correspond to various types of oblique solutions. Finally, the dot-dot-dashed curves (green online) marked by C_1 and $C_{3/2}$ represent solutions of large surface modulation that have no counterpart in the case of flat films (cf. Fig. 9). The fine solid lines (black online) are hypothetical connections that shall serve as a guide to the eye. For details see main text.

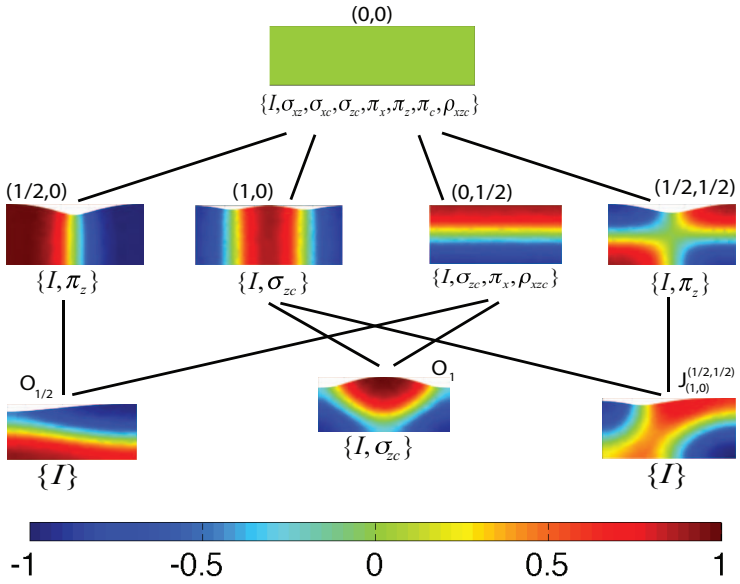

FIG. 24. For the case of films of thickness $H = 5$ without energetic bias and with height modulations, we show (i) typical steady concentration profiles on the various branches in the bifurcation diagram of Fig. 23, (ii) the corresponding symmetries (excluding translations, see main text), and (iii) the relations between the branches. The concentration profiles on the second row are on branches (from the left): (1/2, 0), (1, 0), (0, 1/2), and (1/2, 1/2) all for $L = 10$, whereas the ones on the third row are on branches (from the left) $O_{1/2}$ at $L = 7$, O_1 at $L = 10$, $J^{(1/2,1/2)}_{(1,0)}$ that joins (1, 0) and (1/2, 1/2) at $L = 9$. For remarks on symmetries and line styles, see caption of Fig. 16.

respectively, one notes that it is rather difficult to discern differences to the case of a flat surface (Fig. 9). All branches discussed in Fig. 9 are also present in Fig. 23 with slightly larger norm $||\delta c||$ and slightly lower energy. Now all these solutions have acquired a surface deflection that for the laterally structured solutions increases monotonically with L, but behaves non-monotonically for the various branches of oblique solutions [Fig. 23(c)].

The most important qualitative change is the appearance of solutions with large surface modulation that have no counterpart in the case of flat surfaces. In Fig. 23, they are marked by the dot-dot-dashed (green online) lines, that we name C_1 and $C_{3/2}$. In terms of $||\delta c||$ and E, they stay rather close to other already known branches (what makes their numerical detection rather cumbersome). However, they are strikingly different in terms of $||\delta h||$: The surface modulation strongly increases with L. For instance, one part of the C_1 branch emerges at about $L = 8$ from the O_1 branch, then continues till $L = 10$ where its surface modulation is more than three times stronger than that of the other branches. There is another part of the C_1 branch that emerges at about $L = 11.7$ also from the O_1 branch. It continues towards smaller L and also reaches at $L = 9$ a $||\delta h||$ about three times larger than that of the other branches. Both branching points on the O_1 branch are period doubling bifurcations seemingly related to the suppression of a coarsening mode of instability, and the two parts of the C_1 branch have the same symmetries.

A schematic is given in Fig. 25. This considerations allow us to deduct that the two parts of the C_1 branch are actually connected via two saddle node bifurcations. The resulting hypothetical branch that we are not able to get with our numerical method is indicated in Fig. 23 by a fine black line that may serve as a guide to the eye. We expect similar behaviour for the $C_{3/2}$ branch that bifurcates from the $O_{3/2}$ branch. It is also remarkable that the C_1 branch is locally the one of lowest energy, when comparing to the other branches involved in the transition [i.e., O_1, (0,1/2), (1,0)]. The agreement between the bifurcation points from the laterally homogeneous solutions and the predictions of the dispersion relation (not shown) is good. However, note that there is some room for interpretation as to where exactly some of the bifurcations are in Fig. 23 as some of the branches approach each other rather slowly [e.g., O_1 and (0, 1/2)].

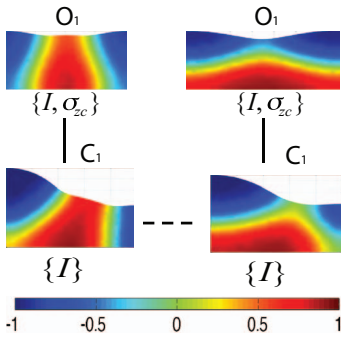

FIG. 25. Shown are further profiles from the branch O_1 and also from the branch C_1 that bifurcates from O_1 shown in Fig. 23. The figure extends Fig. 24. Anti-clockwise, the profiles are on O_1 at $L = 8.2$, on C_1^a at $L = 9$ and $L = 10$, and back on O_1 at $L = 14$. For remarks on symmetries and line styles, see caption of Fig. 16.

Note finally that here as in the case of a flat surface, the absence of an energetic bias implies that most branches are actually two-fold or even four-fold with the different instances being related by the symmetry $c \to -c$ (see Sec. V A). In particular, the "new" large surface modulation C_1 branch is two-fold. This degeneracy is lifted in the case with energetic bias at the free surface that we consider next.

D. Height-modulated films with energetic bias

The fourth and final case we investigate are modulated films with surface bias. Our focus lies on an explanation of the differences to the other cases for the selected film heights $H = 2.5$ and $H = 5.0$. In particular for $H = 5.0$, we restrict our attention to the relatively low energetic bias of $a^+ = 0.1$ because otherwise we are restricted by the convergence of our numerical procedures. This is not the case for the smaller height of $H = 2.5$. There we discuss the case of $a^+ = 0.4$. For much larger energetic bias the surface tension contrast between the two components becomes unphysically large. Even before, at $a^+ = 1/2S$ configurations with three phase contact regions cease to exist in the sharp interface limit.

Even for an imposed flat interface, the liquid-liquid interface is not any more perpendicular to the free surface if an energetic bias is considered. If the free surface is free to move, three curved interfaces meet in the three phase contact region. Note that in the sharp interface limit, one can estimate the angles θ_1 and θ_2 between the diffuse interface and the parts of the free surface where fluid 1 and 2 dominate, respectively. They are given above in Eqs. (15) and (16). For $S = 1$ and $a^+ = 0.1$, one has approximately $\theta_1 = 2.26$ and $\theta_2 = 1.91$, values that well agree with the angles seen in Figs. 29 and 30 below. At $a^+ = 0.4$, $\theta_1 = 2.76$ and $\theta_2 = 1.04$ in rough agreement with Fig. 27 below (note that the measured angles will approach the sharp interface limit as the system size is increased).

1. Films of small thickness (H = 2.5)

The bifurcation diagram for $H = 2.5$ for height-modulated films with an energetic bias of $a^+ = 0.4$ is given in Fig. 26. A selection of corresponding profiles, their symmetry groups and relations between them is given in Fig. 27. Dispersion relations for various a^+ can be found in Fig. 22. Compared to the other cases with $H = 2.5$, an energetic bias of $a^+ = 0.4$ leads to significant changes in the film profiles. The horizontal dot-dashed line in Fig. 26 corresponds to the weakly stratified state (for a profile see first row of Fig. 27) that is unstable with respect to lateral perturbations for $L > L_{1/2}^{\mathrm{ls}} \approx 3.7$. This value results from the linear stability analysis: The dispersion relation for $a^+ = 0.4$ in Fig. 22 gives $k_c = 0.85$ implying the laterally structured (1, 0) branch bifurcates at about $L_1^{\mathrm{ls}} = 7.4$. However, a close inspection of the laterally structured branches indicates that they end at an L slightly smaller than the respective L_c with an amplitude larger than zero. This indicates that the primary bifurcations are subcritical and a very short unstable branch is missing from our

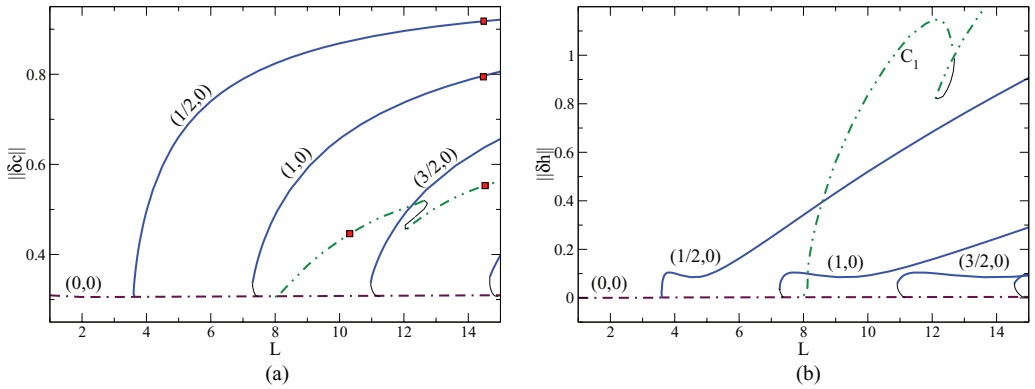

FIG. 26. The bifurcation diagram for steady modulated films for energetic bias $a^+ = 0.4$ and $H = 2.5$ in dependence of the domain size L. Shown are (a) the norm $||\delta c||$, and (b) the norm $||\delta h||$. The dot-dashed horizontal line (maroon online) corresponds to the $(0, 0)$ branch, the solid lines (blue online) are the laterally structured $(s, 0)$ branches, and the dot-dot-dashed lines (green online) represent the C_1 branch of solutions with strong surface modulations (layered drops). The fine solid lines (black online) are hypothetical connections that are discussed in the main text. The symbols indicate profiles shown in Fig. 27.

bifurcation diagram; we sketch its hypothetical location as a fine solid line. Note that the energetic bias shifts all primary bifurcations towards larger L, in good agreement to the dispersion relations (Fig. 22, cf. also Fig. 20). Remarkably, the surface deflection does not increase monotonically along the $(s, 0)$ branches. From the saddle-node bifurcation, it first increases rapidly, then goes slightly down again, before increasing nearly linearly (Fig. 26(b)). Examples for profiles on the laterally structured branches can be found on the second row of Fig. 27.

Another major difference is the appearance of a branch C_1 of solutions (dot-dot-dashed (green online) lines in Fig. 26) with large surface modulation similar to the ones described for modulated films of medium height without bias (see Figs. 23 and 25). Here, however, they are not related to any oblique O_i branch as there exists none. Our hypothesis is that they are related to the "oblique"

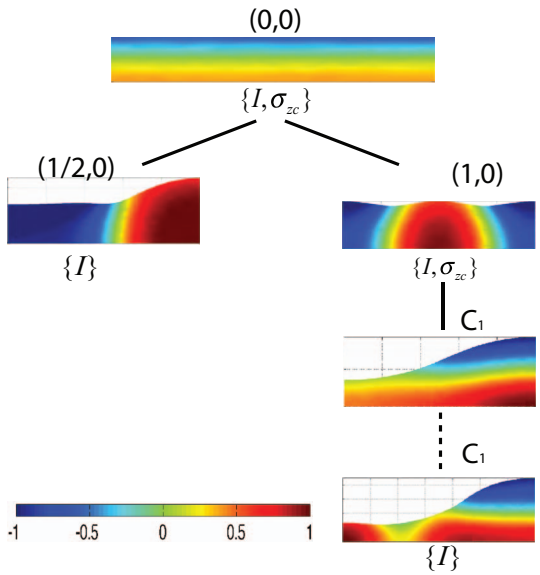

FIG. 27. For the case of height modulated films of thickness $H = 2.5$ with energetic bias $a^+ = 0.4$, we show (i) typical steady concentration profiles from the (0, 0), (1/2, 0), (1, 0) and C_1 branches in Fig. 26 (indicated there by small symbols), and (ii) the corresponding symmetries (excluding translations) and (iii) the relations between the branches. The concentration profiles for the (1/2, 0) and (1, 0) branch are at $L = 14$. For the branch C_1 they are at $L = 10$, and $L = 14$. For remarks on symmetries and line styles, see caption of Fig. 16.

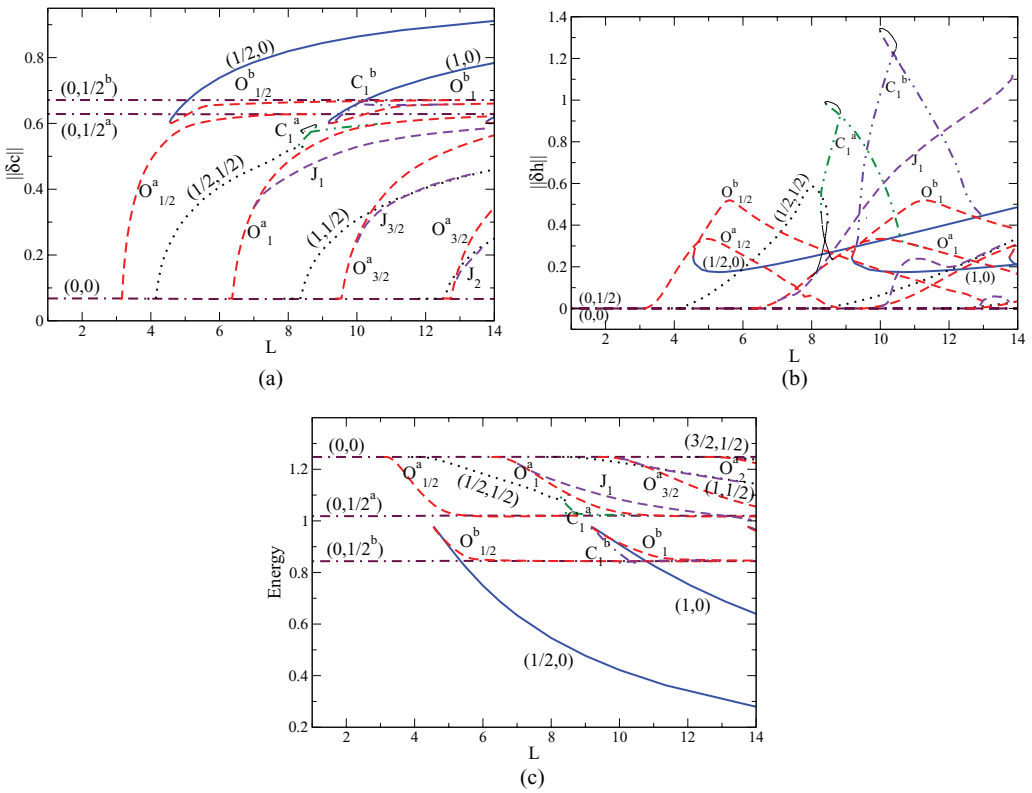

FIG. 28. Bifurcation diagram for modulated film solutions with energetic bias $a^+ = 0.1$ for $H = 5.0$ as function of the domain size L. Shown are (a) the norm $||\delta c||$, and (b) the norm $||\delta h||$. The dot-dashed horizontal lines (maroon online) correspond to the laterally homogenous $(0, n)$-solutions for $n = 0$ (dash-dash-dot) and $n = 1/2$ (dash-dot); the solid lines (blue online) are laterally structured $(s, 0)$-states for $s = 1/2, 1$; the dotted lines (black online) are checker-board $(s, 1/2)$-states for $s = 1/2, 1$; the dashed lines (red and purple online) correspond to various types of oblique solutions. Finally, the dot-dot-dashed curves (green and purple online) marked by C_1^a and C_1^b represent solutions of large surface modulation that do not exist for flat films (cf. Fig. 15). The fine solid lines (black online) are hypothetical connections that are explained in the main text.

solutions on the subcritical piece of the (1, 0) branch that we could not obtain. Considering the symmetries of the solutions (Fig. 27) and the dispersion relation (Fig. 22) that only indicates one instability mode, it seems clear that the C_1 branch does not emerge from the "weakly" modulated (0, 0) branch. Most probably it emerges from the laterally structured (1, 0) branch in a period doubling bifurcation close to the primary bifurcation. This particular feature is better visible for $H = 3.5$ (not shown, see Ref. 35). We expect that the (1, 0) branch beyond this period doubling bifurcation is stable with respect to coarsening. This is remarkable as it is an effect that only appears due to the possible modulation of the free surface, i.e., it is due to the coupling of two rather different degrees of freedom. However, at this point the effect remains hypothetical. Reduced models are needed to investigate it further. On the C_1 branch the surface modulation strongly increases with L. It seems to undergo two further saddle-node bifurcations at about $L = 12$ where we introduce a fine black line in Fig. 26 that indicates the hypothetic connection of the two parts of the C_1 branch that we have determined.

In Fig. 27, relations between the various branches are indicated as solid and dashed straight lines if they are symmetry-breaking pitchfork and not symmetry-breaking saddle-node bifurcations, respectively. As for simplicity we do not include translations in the given scheme, we need to add that in the pitchfurk bifurcation between the (0, 0) and the (1, 0) branch it is actually the translational symmetry T_∞^x that is broken. Note also that all parts of the dot-dot-dashed C_1 branches are connected by saddle-node bifurcations implying that all profiles have the same symmetries.

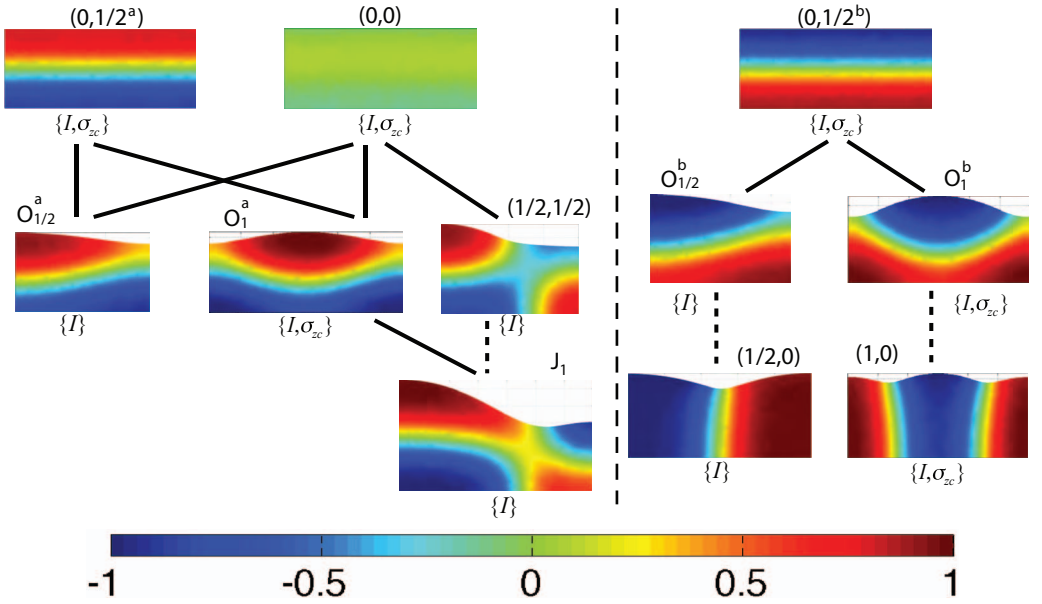

FIG. 29. For the case of modulated films of thickness $H = 5.0$ with energetic bias $a^+ = 0.1$, we show (i) typical steady concentration profiles on the various branches in Fig. 28, (ii) the corresponding symmetries except translations (see main text), and (iii) the relations between the branches. The profiles left (right) of the vertical dashed line belong to the high (low) energy group of solutions. The C_1^i solutions are not included (see Fig. 30). The profiles from the (0, 0), (0, 1/2^a), (0, 1/2^b), (1/2, 0), and (1, 0) branches are for $L = 10$; the $O^a_{1/2}$ and $O^b_{1/2}$ profiles are for $L = 6$ and $L = 7$, respectively; the O^a_1 and O^b_1 profiles are for $L = 12$; the J_1 profile is for $L = 13.5$. For remarks on symmetries and line styles, see caption of Fig. 16.

2. *Films of medium thickness (H = 5.0)*

Finally, we increase the film height to $H > \pi$ where layered solutions become possible, a situation analyzed for modulated films without bias in Sec. V C, and for flat films with bias in Sec. V B. We expect this final most "complex" situation to reflect elements of both these previously studied cases.

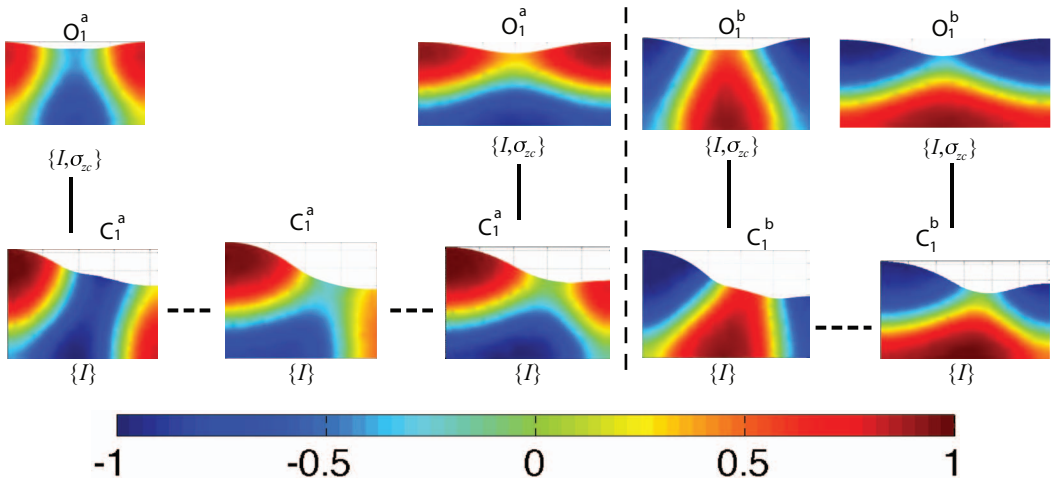

FIG. 30. Shown are profiles from the large surface modulation branches C_1^a and C_1^b that bifurcate from O_1^a and O_1^b, respectively (cf. Fig. 28). Left of the vertical dashed line, we show anticlockwise from top left profiles from O_1^a at $L = 8$, C_1^a at $L = 8.4$ (left half of branch), $L = 8.4$ (right half of branch) and 9.7, and from O_1^a at $L = 12$. Right of the vertical line, we show anticlockwise from the top left profiles from O_1^b at $L = 9.1$, C_1^b at $L = 9.7$ and 12.2. and finally O_1^b at $L = 14.5$. The middle profile In the second row on the left hand side is from a point close to the saddle node bifurcation and illustrates the transition between the two neighboring profiles. For remarks on symmetries and line styles, see caption of Fig. 16.

The bifurcation diagram for $H = 5.0$ for height-modulated films with a small energetic bias of $a^+ = 0.1$ is given in Fig. 28, whereas a selection of corresponding profiles, their symmetry groups and relations between them are given in Figs. 29 and 30. For dispersion relations for the various stratified solutions we refer the reader to Ref. 35.

A first inspection of Fig. 28(a), i.e., the bifurcation diagram in terms of $||\delta c||$ shows that the basic structure is similar to Fig. 15. All layered [(0, 0), (0, $1/2^a$), (0, $1/2^b$)], laterally structured (s, 0), and oblique [O_s^a, O_s^b] branches behave qualitatively similar. A quantitative comparison is not possible as Fig. 28 is for $a^+ = 0.1$ while Fig. 15 is for $a^+ = 0.2$. In the case of modulated free surface for $a^+ = 0.2$, we are not able to obtain all parts of all the branches presented in Fig. 28 due to numerical convergence problems. However, from the partial results we have, one deducts that in the case with surface modulation, secondary bifurcations are shifted to slightly larger L, the norms (energies) of all these branches are slightly higher (lower) than in the case of a flat surface, in accordance to previous observations. All solutions have acquired a surface deflection [Fig. 28(b)]. For the laterally structured solutions (s, 0), it increases monotonically after a small decrease near the saddle-node bifurcation where the (s, 0) branches emerge together with the O_s^b branches. However, most other branches behave non-monotonically.

Comparing with the case of a modulated film without bias (Fig. 23), one notices that again there are solutions with large surface modulation present that do not exist for flat surfaces. In Fig. 28, they are marked by the dot-dot-dashed (green and purple online) lines. There are two sets of them that we name C_1^a (green) and C_1^b (purple). Both result through the breaking of the $c \to -c$ symmetry from the (two-fold) C_1 branch in the case without energetic bias (cf. Fig. 23). As before, they stay rather close to other already known branches in terms of $||\delta c||$ and E. Their surface modulation strongly increases in a small range of L. The C_1^b reaches the largest amplitudes. The various pieces of the C_1^a and C_1^b branches emerge from the O_1^a and O_1^b branches, respectively. All related branching points on the O_1^i branches ($i = a, b$) are period doubling bifurcations related to the suppression of a coarsening mode of instability. The two respective parts of the two C_1^i branches ($i = a, b$) have the same symmetries, as schematically shown in Fig. 30. Again we deduct that the pieces of the C_1^i branches are actually connected via two saddle node bifurcations. The resulting hypothetical branch is indicated in Fig. 28 by a fine black line.

Another important qualitative change is related to the checkerboard solutions [see (1/2, 1/2) branch]. Without energetic bias (Fig. 23), they continue to large L. However, we know already from the case of flat films that an energetic bias results in a re-connection with some of the J branches (see Sec. V B). The effect is visible more clearly here: The (1/2, 1/2) branch emerges at about $L = 4.2$ from the weakly stratified branch. Then its surface deflection increases till $L \approx 8$ where it starts to decrease quickly, passes a saddle-node and joins the O_1^a branch at slightly lower L. We have not been able to obtain the small subcritical part of the branch numerically and indicate its hypothetical path by a fine black line in Fig. 28. Increasing the energetic bias makes the behaviour more pronounced and shifts the subcritical connection of the checkerboard to the oblique branch towards larger L (Ref. 35).

Note finally that in Fig. 29 some of the solutions seem to have the same symmetries although they are connected by a symmetry-breaking pitchfork bifurcation. This results from the exclusion of translational symmetries from our schemes. In particular, the transitions from the (0, 0) to the O_1^a branch, and from the (0, $1/2^b$) to the O_1^b branch, both break the translational symmetry T_∞^x.

With this we end the presentation of our results for the four selected cases, i.e., flat and modulated films with and without energetic bias at the free surface. Section VI concludes, situates our results in the wider context and gives an outlook onto future work.

VI. CONCLUSIONS

We have studied the two-dimensional steady concentration and film thickness profiles for isothermal free surface films of a binary liquid mixture on a solid substrate. They are described by the steady limit of model-H that couples the diffusive transport of the components of the binary mixture (convective Cahn-Hilliard equation) and the transport of momentum (Navier-Stokes-Korteweg equations). Additionally, we have analyzed the linear stability (in time) of relevant stratified (layered) films. This has allowed for a comparison of the position of certain branching points in the

bifurcation diagrams with the value predicted by the linear analysis. The present work forms part three of a sequence of papers, where the first one developed the implemented model and analyzed one-dimensional layered states,[15] whereas the second one introduced the linear stability analysis and applied it to selected layered states for a number of different types of energetic biases at *both* interfaces.[17]

The present study has restricted itself to the case of asymmetric bias, i.e., the solid substrate has been taken as energetically neutral, while an energetic bias has been applied at the free surface that corresponds to a linear solutal Marangoni effect. For comparison, we have also studied the case without any energetic bias. Our particular attention has been focused on the transitions that occur when one goes from a film with an imposed free surface to one where the free surface is able to deform.

After a brief recapitulation of the non-dimensional model-H, the appropriate boundary conditions, the linearization of the fully time-dependent equations about the stratified steady films and the employed numerical schemes, we have discussed the linear stability of the homogeneous films and the one-dimensional (layered) films that are relevant for the present work. Based on this, we have then analyzed the fully two-dimensional steady films. Results obtained in the form of bifurcation diagrams of the various steady states and particular concentration and thickness profiles have been related to the linear results obtained before. In particular, we have presented results for the cases of (i) a flat film without energetic bias at the free surface (Sec. V A), (ii) a flat film with energetic bias (Sec. V B), (iii) a height-modulated film without energetic bias (Sec. V C), and (iv) a height-modulated film with energetic bias (Sec. V D). All cases have been studied for a number of film thicknesses and (if applicable) energetic biases.

In general, we find that the complexity of the bifurcation diagrams increases with increasing film thickness and lateral domain size, as one would expect from the linear stability of a homogeneous film as an increasing number of modes becomes unstable. Based on this observation we have distinguished "thin films" ($0 < H < \pi$) where the homogeneous film is only unstable with respect to lateral modes, "medium films" ($\pi \leq H < 2\pi$) where additionally the first vertical structuring mode is unstable, and "thick films" ($2\pi \leq H$) where more vertical modes are unstable. We have not pursued an analysis of the thick films as the picture becomes rather involved and main results are already obtained with medium films. Similarly, in the cases with surface modulation we have restricted the study to relatively small energetic bias, while for flat films it has been possible to also study higher biases.

Even for thin and medium films, the bifurcation diagrams can be quite involved. For instance, in the case of flat films of medium thickness without energetic bias we have found a number of different laterally structured films, layered films, checkerboard films and obliquely structured films (Sec. V A). We have analyzed the symmetries of the steady solutions on the individual branches and have employed ideas from equivariant bifurcation theory to discuss the relations between the branches. This has allowed us to infer the multiplicity of the various branches, their linear stability, and the character of the symmetry breaking bifurcations. Note, however, that to sort our results we merely use a selection of symmetry operations that may be applied to the steady film solutions (reflections, inversions and rotations in a space spanned by the spatial coordinates and the concentration). To keep the picture simple, we have whenever possible excluded translations. A proper group theoretical treatment is beyond the scope of the present work.

The symmetry considerations have been helpful in the cases with energetic bias and/or surface modulation, in particular, close to some of the bifurcations where the achievable numerical precision does not allow us to decide which branches are actually connected. In all these cases, arguments based on symmetries made it possible to clearly determine the bifurcational structure. This has been particularly important in the case of modulated surfaces where the additional degree of freedom results in the appearance of a new type of solution—large amplitude layered drops that result from a coarsening or period doubling bifurcation.

Beside the steady states, we have investigated the linear stability (in time) of the layered films. In general, we have found a good agreement of the loci of the relevant bifurcations. However, in a few cases the various branches are already very close to each other far away from the bifurcation points and our numerical scheme does not allow for an exact determination of the bifurcation point. Nevertheless, we conclude that the two different numerical approaches—linear stability analysis of

layered solutions within the fully time-dependent model-H and determination of steady states via a minimization of the underlying energy functional—agree rather well.

Inspecting all the obtained solutions for various energetic biases, film thicknesses and domain sizes one notices that the energetically favoured solution is nearly always the laterally structured one. This is mainly due to the setup of our study: we have chosen an energetically neutral substrate to focus on the effect of an energetic bias at the free surface. Compare Ref. 34 for an example with an energetic bias at the substrate but a neutral free surface. Furthermore, we have chosen to study a symmetrical blend (critical case) where the mean concentration of the two components are equal. A study of the case of non-symmetric blends (off-critical) will be considered elsewhere. Another important restriction is our focus on a linear energetic bias. Other parameters have stayed fixed throughout our study as, e.g., the ratio of the surface tension of the liquid-gas interface and the one of the internal diffuse interface. Without doubt, some of the possible changes in the setup will energetically favour other solutions than the laterally structured one. We expect our results to be also useful for future studies of similar systems as the basic bifurcational structures discussed here will reflect aspects of such structures in other cases.

A further limitation of the present study is our restriction to a two-dimensional geometry. This implies that, e.g., the two-dimensional droplets in all shown concentration profiles actually represent cuts through ridges that are invariant with respect to translations into the third dimension (y-coordinate). Such ridges might be unstable to a Plateau-Rayleight instability[45,46] if the domain size in y-direction passes a critical value. This possibility will further enrich the bifurcation diagrams as it might, e.g., result in coexistence regions of ridge and 3D drop states resulting from a subcritical instability of the ridges with respect to transversal perturbations as observed, for instance, for liquid ridges on homogeneous and heterogeneous solid substrates.[47] However, the present approach might become rather involved in the general three-dimensional case. Therefore, a reduced description for practically important cases should be sought. A possible option is described in the next and final paragraph.

The present study has shown that for the chosen parameter values laterally structured films are normally the energetically favourable solution. This indicates that for these parameter values one should be able to derive an asymptotic model that focuses on the lateral aspects, i.e., "slaves" the vertical concentration profile to effective fields that only depend on the lateral coordinate. Such a description was derived recently through a long-wave approximation of model-H[20] and consists of coupled evolution equations for the vertically averaged concentration and the film thickness profile. Their model may also be directly obtained as an extension of a gradient dynamics formulation of thin film hydrodynamics for a film of suspension, blend or solution as shown in Ref. 21. Related models are also developed in Ref. 19. For the future, direct simulations of the dynamics of such films as obtained with model-H should be compared to results for the time evolution obtained with the different proposed long-wave (or thin film) models.

ACKNOWLEDGMENTS

This work was supported by the European Union under Grant No. PITN-GA-2008-214919 (MULTIFLOW). F.B. thanks the Libyan Ministry of Higher Education for a personal grant. The authors thank A. J. Archer, L. Frastia, E. Knobloch, and S. Madruga for many useful discussions, and L. Frastia for help with the FEM code.

[1] K. G. Winkels, I. R. Peters, F. Evangelista, M. Riepen, A. Daerr, L. Limat, and J. H. Snoeijer, "Receding contact lines: From sliding drops to immersion lithography," Eur. Phys. J. Spec. Top. **192**, 195–205 (2011).
[2] J. Heier, J. Groenewold, F. A. Castro, F. Nüesch, and R. Hany, "Enlarged bilayer interfaces from liquid-liquid dewetting for photovoltaic applications," *Organic Optoelectronics and Photonics III*, edited by P. L. Heremans, M. Muccini, E. A. Meulenkamp, Proc. of SPIE Vol. 6999, 69991J (2008).
[3] G. S. Hwang, M. Kaviany, J. H. Nam, M. H. Kim, and S. Y. Son, "Pore-water morphological transitions in polymer electrolyte of a fuel cell," J. Electrochem. Soc. **156**, B1192–B1200 (2009).
[4] C. E. Colosqui, M. J. Cheah, I. G. Kevrekidis, and J. B. Benziger, "Droplet and slug formation in polymer electrolyte membrane fuel cell flow channels: The role of interfacial forces," J. Power Sources **196**, 10057–10068 (2011).
[5] M. Geoghegan and G. Krausch, "Wetting at polymer surfaces and interfaces," Prog. Polym. Sci. **28**, 261–302 (2003).

[6] K. R. Thomas, N. Clarke, R. Poetes, M. Morariu, and U. Steiner, "Wetting induced instabilities in jciteible polymer blends," Soft Matter **6**, 3517–3523 (2010).
[7] X. Bulliard, S.-G. Ihn, S. Yun, Y. Kim, D. Choi, J.-Y. Choi, M. Kim, M. Sim, J.-H. Park, W. Choi, and K. Cho, "Enhanced performance in polymer solar cells by surface energy control," Adv. Funct. Mater. **20**, 4381–4387 (2010).
[8] J. You, Y. Liao, Y. Men, T. Shi, and L. An, "Film thickness dependence of phase separation and dewetting behaviors in PMMA/SAN blend films," Langmuir **26**, 14530–14534 (2010).
[9] P. G. Nicholson and F. A. Castro, "Organic photovoltaics: Principles and techniques for nanometre scale characterization," Nanotechnology **21**, 492001 (2010).
[10] M. Ramanathan and S. B. Darling, "Mesoscale morphologies in polymer thin films," Prog. Polym. Sci. **36**, 793–812 (2011).
[11] A. Sharma and R. Khanna, "Pattern formation in unstable thin liquid films," Phys. Rev. Lett. **81**, 3463–3466 (1998).
[12] U. Thiele, "Thin film evolution equations from (evaporating) dewetting liquid layers to epitaxial growth," J. Phys. Condens. Matter **22**, 084019 (2010).
[13] D. Bonn, J. Eggers, J. Indekeu, J. Meunier, and E. Rolley, "Wetting and spreading," Rev. Mod. Phys. **81**, 739–805 (2009).
[14] R. Yerushalmi-Rozen, T. Kerle, and J. Klein, "Alternative dewetting pathways of thin liquid films," Science **285**, 1254–1256 (1999).
[15] U. Thiele, S. Madruga, and L. Frastia, "Decomposition driven interface evolution for layers of binary mixtures: I. Model derivation and stratified base states," Phys. Fluids **19**, 122106 (2007).
[16] O. A. Frolovskaya, A. A. Nepomnyashchy, A. Oron, and A. A. Golovin, "Stability of a two-layer binary-fluid system with a diffuse interface," Phys. Fluids **20**, 112105 (2008).
[17] S. Madruga and U. Thiele, "Decomposition driven interface evolution for layers of binary mixtures: II. Influence of convective transport on linear stability," Phys. Fluids **21**, 062104 (2009).
[18] A. Oron, S. H. Davis, and S. G. Bankoff, "Long-scale evolution of thin liquid films," Rev. Mod. Phys. **69**, 931–980 (1997).
[19] N. Clarke, "Toward a model for pattern formation in ultrathin-film binary mixtures," Macromolecules **38**, 6775–6778 (2005).
[20] L. Ó. Náraigh and J. L. Thiffeault, "Nonlinear dynamics of phase separation in thin films," Nonlinearity **23**, 1559–1583 (2010).
[21] U. Thiele, "Note on thin film equations for solutions and suspensions," Eur. Phys. J. Spec. Top. **197**, 213–220 (2011).
[22] A. Pototsky, M. Bestehorn, D. Merkt, and U. Thiele, "Morphology changes in the evolution of liquid two-layer films," J. Chem. Phys. **122**, 224711 (2005).
[23] L. S. Fisher and A. A. Golovin, "Nonlinear stability analysis of a two-layer thin liquid film: Dewetting and autophobic behavior," J. Colloid Interface Sci. **291**, 515–528 (2005).
[24] D. Bandyopadhyay, R. Gulabani, and A. Sharma, "Stability and dynamics of bilayers," Ind. Eng. Chem. Res. **44**, 1259–1272 (2005).
[25] P. C. Hohenberg and B. I. Halperin, "Theory of dynamic critical phenomena," Rev. Mod. Phys. **49**, 435–479 (1977).
[26] D. M. Anderson, G. B. McFadden, and A. A. Wheeler, "Diffuse-interface methods in fluid mechanics," Annu. Rev. Fluid Mech. **30**, 139–165 (1998).
[27] D. Jasnow and J. Viñals, "Coarse-grained description of thermo-capillary flow," Phys. Fluids **8**, 660–669 (1996).
[28] J. Lowengrub and L. Truskinovsky, "Quasi-incompressible Cahn-Hilliard fluids and topological transitions," Proc. R. Soc. London, Ser. A **454**, 2617–2654 (1998).
[29] N. Vladimirova, A. Malagoli, and R. Mauri, "Two-dimensional model of phase segregation in liquid binary mixtures," Phys. Rev. E **60**, 6968–6977 (1999).
[30] N. Vladimirova, A. Malagoli, and R. Mauri, "Diffusion-driven phase separation of deeply quenched mixtures," Phys. Rev. E **58**, 7691–7699 (1998).
[31] R. Borcia, D. Merkt, and M. Bestehorn, "A phase-field description of surface-tension-driven instability," Int. J. Bifurcation Chaos **14**, 4105–4116 (2004).
[32] R. Borcia and M. Bestehorn, "Different behaviors of delayed fusion between drops with jciteible liquids," Phys. Rev. E **82**, 036312 (2010).
[33] J. W. Cahn, "Phase separation by spinodal decomposition in isotropic systems," J. Chem. Phys. **42**, 93–99 (1965).
[34] L. Frastia, U. Thiele, and L. M. Pismen, "Determination of the thickness and composition profiles for a film of binary mixture on a solid substrate," Math. Model. Nat. Phenom. **6**, 62–86 (2011).
[35] F. Bribesh, *Free Surface Films of Binary Liquid Mixtures* (Loughborough University, Loughborough, 2012).
[36] D. J. Korteweg, "Sur la forme que prennent les équations du mouvement des fluides si l'on tient compte des forces capillaires causées par des variations de densité," Arch. Néerl. Sci. Exactes Nat., Ser. II **6**, 1–24 (1901).
[37] J. W. Cahn and J. E. Hilliard, "Free energy of a nonuniform system. 1. Interfacual free energy," J. Chem. Phys. **28**, 258–267 (1958).
[38] J. D. Crawford, M. Golubitsky, M. G. M. Gomes, E. Knobloch, and I. M. Stewart, "Boundary conditions as symmetry constraints," in *Singularity Theory and Its Applications, Part II*, Lecture Notes in Mathematics Vol. 1463 (Springer, New York, 1991), pp. 63–79.
[39] K.-J. Bathe, *Finite Element Procedures*, 2nd ed. (Prentice-Hall, New Jersey, 1995).
[40] E. J. Doedel, R. C. Paffenroth, A. R. Champneys, T. F. Fairgrieve, Y. A. Kuznetsov, B. E. Oldeman, B. Sandstede, and X. J. Wang, *AUTO2000: Continuation and Bifurcation Software for Ordinary Differential Equations* (Concordia University, Montreal, 1997).
[41] R. Kenzler, F. Eurich, P. Maass, B. Rinn, J. Schropp, E. Bohl, and W. Dieterich, "Phase separation in confined geometries: Solving the Cahn-Hilliard equation with generic boundary conditions," Comput. Phys. Commun. **133**, 139–157 (2001).
[42] J. D. Crawford and E. Knobloch, "Symmetry and symmetry-breaking bifurcations in fluid-dynamics," Annu. Rev. Fluid Mech. **23**, 341–387 (1991).
[43] R. B. Hoyle, *Pattern Formation – An Introduction to Methods* (Cambridge University Press, Cambridge, 2006).

[44] Note that the group is not strictly complete as translations are not included. It is pointed out in Ref. 38 that any solution on a domain with von Neumann boundary conditions (NBC) may be extended by reflection to a solution with periodic boundary conditions (PBC) on twice the domain size. With other words NBC may be considered as symmetry constraint on the problem with PBC that is invariant under $\mathbf{O(2)}^x \times \mathbf{Z}_2^z \times \mathbf{Z}_2^c$. For our case, this implies that solutions of a lateral mode number s are in the extended system invariant under translations $\mathbf{T}_{L/s}$: $x \to x + L/s$ (note that the mode number definition in Ref. 38 differs from ours. The additional symmetry results from the embedding of the NBC system in a PBC system but is not a symmetry of the original equations with NBC. A similar argument holds for the z-direction in the case of a flat film without energy bias at the free surface, i.e., Eq. (6) becomes $\partial_z c = 0$ and the symmetry of the problem is $\mathbf{O(2)}^x \times \mathbf{O(2)}^z \times \mathbf{Z}_2^c$. This subtle issue has consequences for the overall bifurcational structure, e.g., the primary bifurcations with respect to lateral modes with $s = 1/2$ and vertical modes with $n = 1/2$ become pitchfork bifurcations where the two half-branches are identified (in the extended PBC domain) by T_L: $x \to x + L$ and T_H: $x \to x + H$, respectively. For the underlying theory, see Ref. 38.

[45] S. H. Davis, "Moving contact lines and rivulet instabilities. Part 1. The static rivulet," J. Fluid Mech. **98**, 225–242 (1980).

[46] M. Grinfeld, "On the Plateau-Rayleigh instability of truncated cylinder," Mech. Res. Commun. **21**, 613–616 (1994).

[47] P. Beltrame, E. Knobloch, P. Hänggi, and U. Thiele, "Rayleigh and depinning instabilities of forced liquid ridges on heterogeneous substrates," Phys. Rev. E **83**, 016305 (2011).